Available online at www.sciencedirect.com
SCIENCE DIRECT
Planetary and Space Science 54 (2006) 219–242
Planetary and Space Science
www.elsevier.com/locate/pss

# New observations of Warrego Valles, Mars: Evidence for precipitation and surface runoff

V. Ansan*, N. Mangold

*Laboratoire IDES - UMR 8148-CNRS, Université Paris-Sud, bât. 509, 91405 Orsay Cedex, France*

Received 25 August 2004; received in revised form 11 July 2005; accepted 12 December 2005

**Abstract**

Most valley networks have been identified primarily in the heavily cratered uplands which are Noachian in age (>3.5 Gyr). A striking exception to this general observation is Warrego Valles located on the southeastern part of the Tharsis bulge. Recent data obtained by the Mars Orbiter Laser Altimeter, the Thermal Emission Imaging System (THEMIS) spectrometer and the Mars Orbiter Camera give new insight into the formation of valley networks and the early Mars climate. We focus our study on the southern Thaumasia region especially on Warrego Valles and determine the organisation of valleys in relation to regional topography and structural geology. Warrego Valles is the most mature valley network that incised the southern side of Thaumasia highlands. It developed in a rectangular-shaped, concave-up drainage basin. Four times more valleys are identified in THEMIS infrared images than in Viking images. Valleys exist on both sides of the main tributary contrary to what was visible in Viking images. Their distribution is highly controlled by topographic slope, e.g. there is a parallel pattern on the sides and dendritic pattern on the central part of Warrego Valles. We quantitatively analyse valley morphology and morphometry to determine the processes responsible for valley network formation. Warrego Valles displays morphometric properties similar to those of a terrestrial fluvial valley network. This valley network is characterised by seven Strahler's orders, a bifurcation ratio of 3, a length ratio of 1.7, a drainage density of 0.53 $km^{-1}$ and a ruggedness number of 3.3. The hypsometric curve and integral (0.46) indicate that Warrego Valles reached the mature Davis' stage. Valleys have undergone external degradation since their incision, which masks their main morphological characteristics. Our study supports the assertion that valley networks formed by fluvial processes controlled by an atmospheric water cycle. Further, they seem to develop by successive stages of erosion that occurred during Noachian through the late Hesperian.


*Keywords:* Warrego Valles; Mars; Valley network; Water; Fluvial process; Noachian–Hesperian

## 1. Introduction

Since the Mariner missions, valley networks are found in the heavy cratered uplands south of the Martian dichotomy (Schultz and Ingerson, 1973; Carr and Clow, 1981; Mars Channel Working Group, 1983; Carr, 1995). Valley networks are defined as a set of valleys typically arranged in a dendritic pattern. Because of their similarity with that of terrestrial fluvial valley networks, a variety of processes involving liquid water have been proposed to explain their formation. Such processes include: (1) fluvial erosion by a combination of surface runoff and groundwater sapping (Milton, 1973; Baker and Kochel, 1979; Gulick and Baker, 1989, 1990; Baker et al., 1992; Carr, 1995, 1996; Grant, 2000; Malin and Edgett, 2000; Ansan and Mangold, 2003); (2) groundwater sapping resulting from geothermal or hydrothermal heating (Sharp and Malin, 1975; Pieri, 1976, 1980; Howard, 1988; Squyres, 1989; Baker, 1990; Goldspiel et al., 1993; Gulick, 1998, 2001; Goldspiel and Squyres, 2000; Luo, 2002); (3) groundwater flow associated with chemical and mechanical erosion (Malin and Carr, 1999; Carr and Malin, 2000); and (4) water-lubricated mass wasting (Carr, 1995). Because valley networks are found on the heavily cratered terrains, they probably formed during the late Noachian (>3.5 Gyr). Their formation by liquid water would imply that Mars had a warmer and wetter

*Corresponding author. Fax: +33 1 60 19 14 46.
*E-mail addresses:* ansan@geol.u-psud.fr (V. Ansan), mangold@geol.u-psud.fr (N. Mangold).

0032-0633/$ - see front matter © 2006 Elsevier Ltd. All rights reserved.
doi:10.1016/j.pss.2005.12.009

climate early in its history (Sagan et al., 1973; Carr, 1981; Craddock and Howard, 2002) because liquid water is unstable on the Martian surface under the present-day climatic conditions (Leighton et al., 1965; Farmer and Doms, 1979). The debate continues about climatic conditions on early Mars because numerous climate models argue in favour of a cold and dry climate since ~4 Gyr (Kasting, 1991; Clifford, 1993).

In order to discriminate between the two opposite Martian climatic scenarios, we analysed valley networks located on the southern boundary of the Tharsis bulge in the Thaumasia region (Fig. 1a). This region is characterised by a 4 km high plateau surrounded by highlands rising to an elevation >5 km (Fig. 1b). Numerous folds, faults, rift valleys and volcanoes have been identified (Schultz and Tanaka, 1994; Tanaka et al., 1998; Dohm and Tanaka, 1999; Dohm et al., 2001). These investigations indicated that Thaumasia is ~3.5 Gyr old corresponding to the Noachian epoch (Tanaka, 1986; Dohm and Tanaka, 1999). It is bounded by cratered plains dated from the late Noachian to the early Hesperian in the south (Dohm et al., 2001). The Thaumasia highlands have been dissected by numerous valley networks (Fig. 1a and 1b) which debouch onto the southern plains (Fig. 1a). The valley networks formed from the late Noachian through the early Hesperian (<3.0 Gyr) based on their relative chronology and crater counts from Viking images (Tanaka, 1986; Tanaka et al., 1998; Dohm and Tanaka, 1999). Valley networks display an usually low degree of organisation with few branches in this area, but some of them appear to be more mature, such as Warrego Valles, which is located (42°S–93°W) on a regional south-facing slope on the southern boundary of the Thaumasia region (WR in Fig. 1). Viking images show that Warrego Valles is characterised by a well-formed parallel valley system in which secondary valleys join the main one (Pieri, 1980). It is interpreted to have been formed by surface runoff because of its resemblance to terrestrial fluvial valley systems (Carr, 1981; Baker, 1982, 1985). However, surface runoff is often rejected because of the low drainage density and the low degree of valley organisation of Warrego system (Cabrol and Grin, 2001; Stepinski and Collier, 2003). Alternatively, it has been suggested that groundwater sapping triggered by geothermal or hydrothermal heating (Tanaka et al., 1998; Dohm and Tanaka, 1999; Gulick, 2001) supported by the regional volcanic and tectonic context of Thaumasia highlands, carved the Warrego system.

New data from Mars Global Surveyor and Mars Odyssey allow us to study Warrego Valles in much more detail. These data allow us to test hypothesis regarding the origin of valley networks in this area. Unlike previous studies, we also have topography from the Mars Orbiter Laser Altimeter (MOLA) (Smith, 1998) with a height accuracy of 50 cm. In addition, the surface of Mars has been imaged with spatial resolution ranging from ~100 to few m/pixel by different instruments including the Mars Orbiter Camera (MOC) (Malin et al., 1998) and Thermal Emission Imaging System (THEMIS) which covers visible and thermal infrared (IR) wavelengths (Christensen et al., 2003). By combining these data sets (altimetry, Viking, MOC and THEMIS images) and using standard geospatial analytical techniques that are available in many Geographic Information Systems (GIS), we derived a geologic map of this area in which valleys networks, craters and faults were identified. Our objectives are to: (1) determine the organisation of valleys in relation with the regional topography and structural geology; (2) estimate the age and the duration of the formation of the valley networks; (3) analyse the morphology and the morphometry of Warrego Valles; (4) determine the process(es) for valley network formation; and (5) deduce the climatic conditions in which Warrego Valles and surrounding valley networks formed within the Thaumasia highlands.

## 2. Morphology and age of valley networks

The southern boundary of Thaumasia region has been dissected by numerous valley networks (Fig. 1). The most well-defined network, Warrego Valles, developed in the area between 40° and 44° south, and between 91° and 96° west. We studied the characteristics of the valley network system at different scales, using both MOLA altimetry, and available visible and mid-IR images acquired during the Viking, MGS and Mars Odyssey missions. Each data set was projected on the IAU2000 Mars datum (Duxbury et al., 2002; Seidelmann et al., 2002) with a Lambert conformal projection in GIS (ARCVIEW and Er-mapper). From these data, we mapped the valley networks, impact craters and faults present in the Warrego Valles area in order to define the geologic context in which valley networks formed.

### 2.1. Organisation of valleys in Warrego Valles from imagery at different scales

Warrego Valles was first mapped using Viking image mosaics (MDIM.2, images extracted from PDS web site; Kirk et al., 2001) with a resolution of ~200 m/pixel at 42°S of latitude (Fig. 2). In this mosaic, the Martian surface was illuminated by low sun angles, which enhanced the local ground morphology. We superposed this mosaic on to MOLA altimetry data, interpolated with a spatial resolution of ~463 m/pixel (Zuber et al., 1992; Smith et al., 1999, 2001), to help the geomorphic analysis.

The southern part of the Viking mosaic contains the Hesperian-age plain of Sirenum Terra (Tanaka, 1986; Dohm and Tanaka, 1999) standing at an elevation of 2.4 km. It borders the southern Thaumasia highlands that reach a maximum elevation of 8.8 km (92.7°W–40.5°S) with a 2° south-facing slope. The Thaumasia highlands are cut by three sets of normal faults oriented W–E, NNE–SSW and NNW–SSE, all of which contain long and narrow grabens that crosscut the southern Hesperian plain.

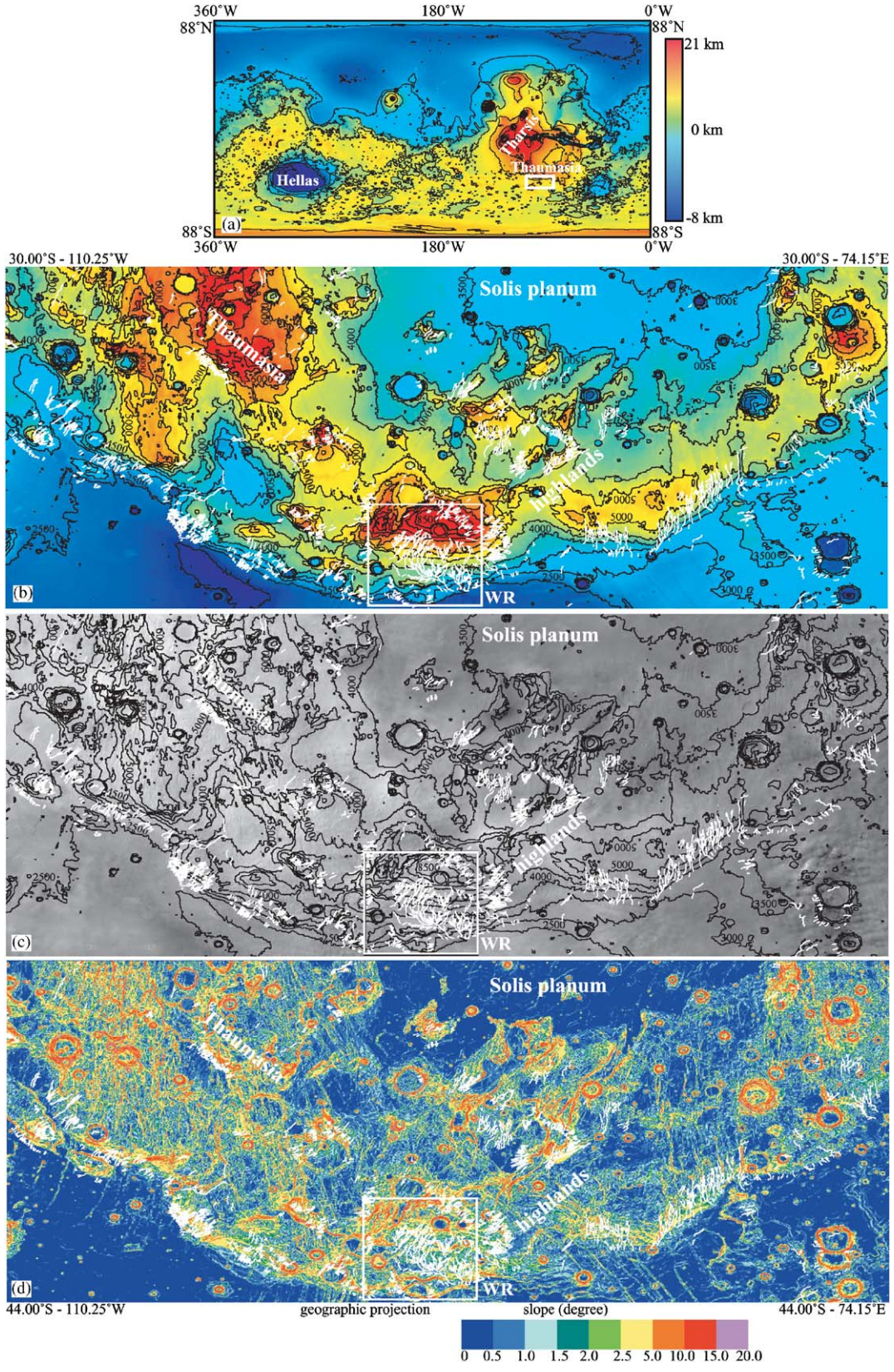


Fig. 1. (a) Topographic map of Mars based on MOLA data. The inner box corresponds to the Thaumasia region located on the southern edge of Tharsis bulge. (b). Topographic map of south Thaumasia region based on MOLA data with contour lines spaced of 500 m height intervals. (c) Mosaic of MOC context images on which MOLA height intervals are plotted. (d) Map of local topographic slopes within south Thaumasia region. The northern plateau and the southern plain are nearly flat (slope $<1.5^{\circ}$). Thaumasia highlands display greater slopes ($<5^{\circ}$) and local topographic scarps associated to fault scarps or crater rims may reach $20^{\circ}$ slopes. On all maps, valley networks are marked by bold white lines. White box annotated WR corresponds to the location of Warrego Valles.

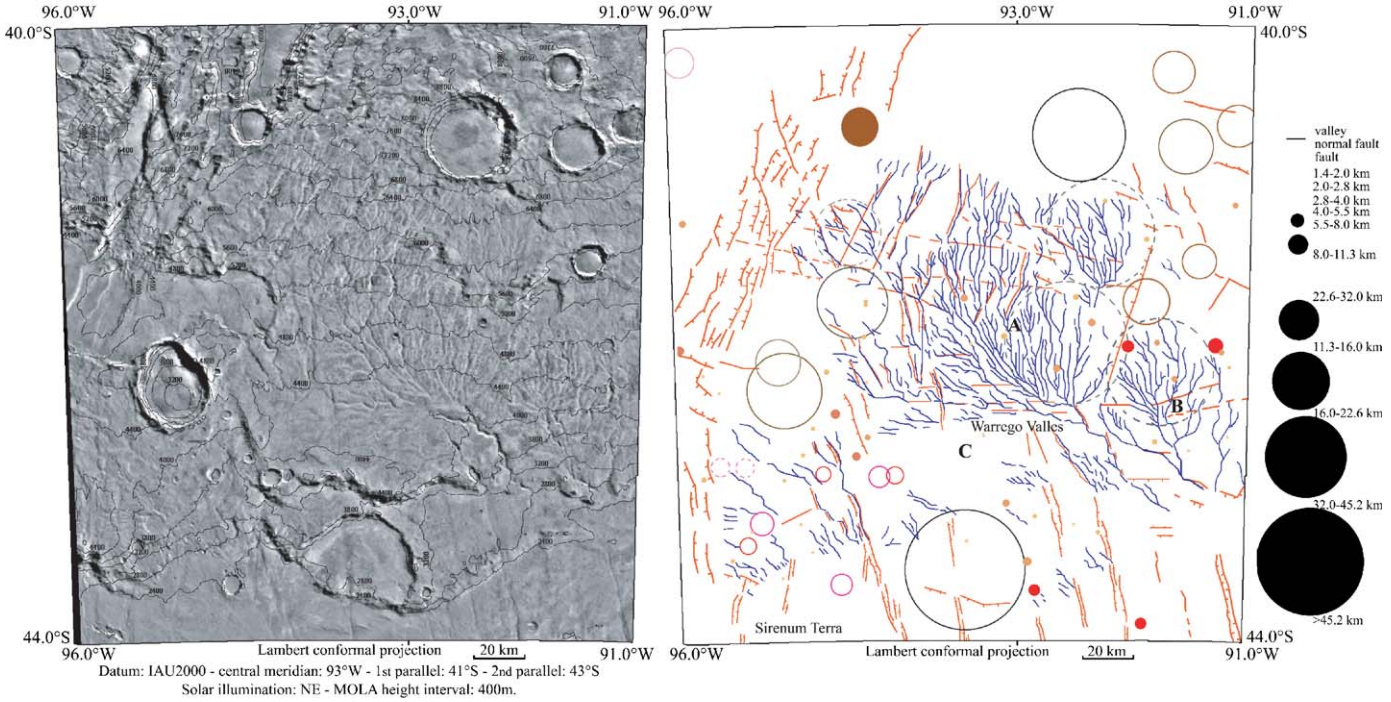


Fig. 2. Mosaic of Viking images (MDIM.2) centred on Warrego Valles, and its geomorphic and geologic map. MOLA height contour lines were superposed on Viking images. Within interpretative map, impact craters are represented with their diameter and their scale of modified morphology: when they are not modified by erosion or infilling, they are indicated by filled circle; when they show an eroded shape, they are marked by an empty circle, and when they appear in highly modified shape, they are drawn by a dashed circle. Points A, B and C are discussed in text.

The south-facing slope of Thaumasia highlands appears dissected by sub-parallel, straight and relatively wide and deep valleys oriented predominantly N–S (Fig. 2) as observed in previous studies (Pieri, 1980; Tanaka et al., 1998; Dohm and Tanaka, 1999; Dohm et al., 2001). The valleys seem to have developed exclusively on the local south-facing slopes, i.e. the south-facing topographic scarp bounding the north part of Sirenum plain. The valleys have a branching-like pattern and show an Earth-like fluvial spatial organisation on the regional highland slope. Two mature valley networks can be observed, including the main Warrego valley network (42°S–93°W, point A in Fig. 2) and a secondary network (42°S–92°W, point B in Fig. 2).

At 1:560,000 Viking scale, the sub-parallel, N–S trending, valleys of Warrego Valles connect to a main orthogonal, W–E trending, wide tributary located at the south where topographic slope decreases. The main tributary shows a regular path with rectangular inflexions suggesting control by tectonic faults. It terminates suddenly at the southeastern toe of the Thaumasia highlands with no alluvial fan. It is important to note that the valley organisation of Warrego Valles appears asymmetrical with all other valleys on the same side of the main tributary. No valley appears to be present on the south side (point C in Fig. 2). Note also that valley heads seem to stand at the same elevation, suggesting that seeping occurred at around 7 km in elevation.

The secondary network (B in Fig. 2) has a 30 km in diameter sub-circular shape, similar to a typical terrestrial drainage basin. Its basin divide may correspond to a rim of an old and filled crater. Valleys show a hierarchical arrangement with larger and larger tributaries to the outlet distributed in a sub-dendritic pattern. Valley heads are distributed at different elevations ranging from 4 to 4.8 km. No alluvial fan is observed at the mouth of drainage basin.

Note also that the valley heads of other networks present in this area are located at different elevations (from 3.5 to 5.5 km), particularly the less mature valley networks on the boundary of Sirenum plain (Fig. 1b and 2). This has been previously observed and mapped from the Viking mosaics at regional scale (Dohm et al., 2001). The location of valley heads at different elevations suggests that there were several water tables perched on top of one another.

Daytime THEMIS IR images give new insights into the organisation of the valley networks in this area. THEMIS has filters centred on nine wavelengths between 6.6 and 15 μm. The signal corresponds to the surface temperature at the resolution of ~100 m which can be related to thermal properties of materials (Christensen et al., 2003). Owing to their time acquisition (3–4 p.m.), the daytime IR thermal signal is dominated by albedo and topographic effects (i.e. southwest-facing slopes are bright at this latitude (Christensen et al., 2003). Images have a spatial resolution of 101 m, which is a good scale to provide an understanding of the regional geological context. The mosaic of daytime

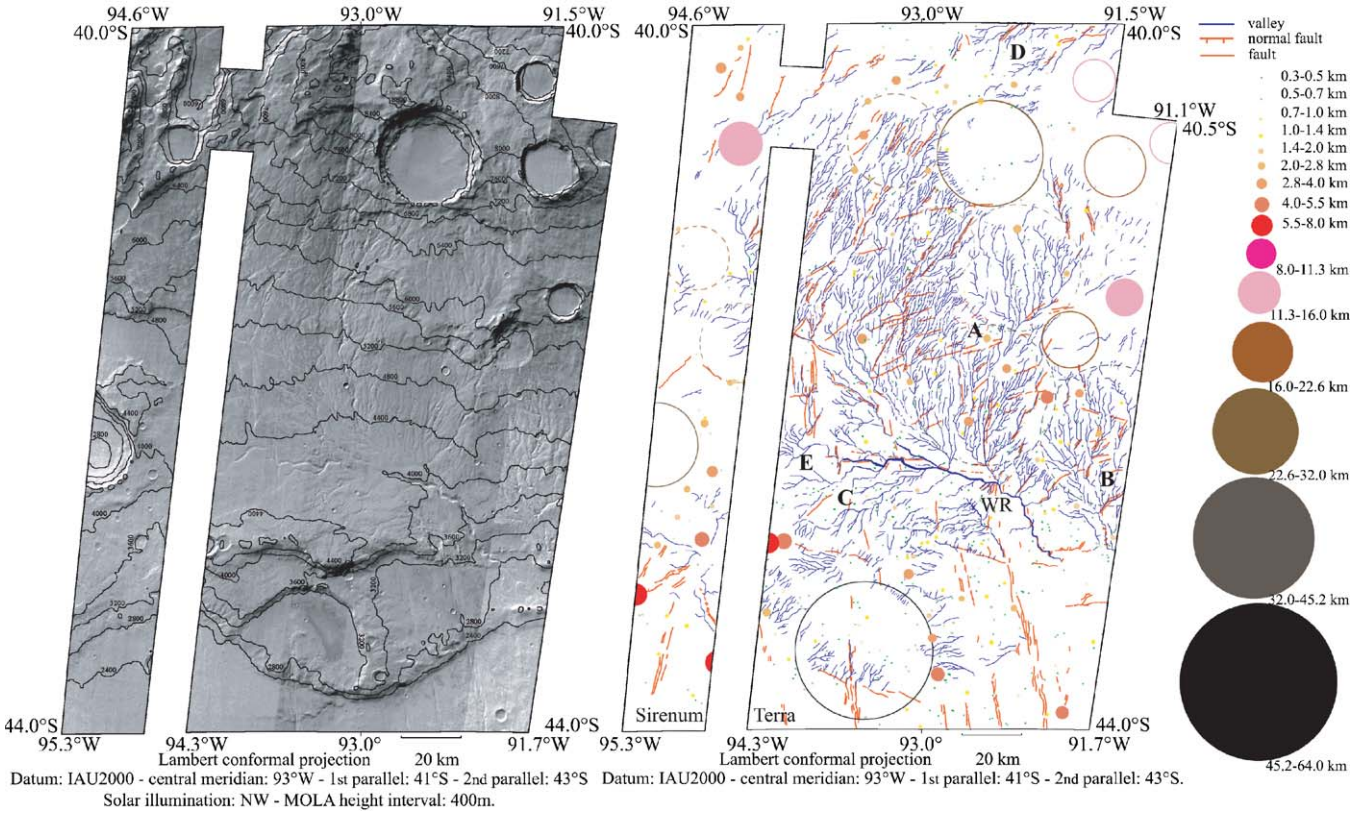


Fig. 3. Mosaic of daytime mid-infrared THEMIS images and its interpretative map centred on Warrego Valles (WR). (from west to east: I05484002, I02463007, I05459002, I01714004, I02800002, I01689003 and I054090002). MOLA height contour lines were superposed on THEMIS images. Within interpretative map, impact craters are represented with their diameter and their scale of modified morphology: when they are not modified by erosion or infilling, they are indicated by filled circle; when they show an eroded shape, they are marked by an empty circle, and when they appear in highly modified shape, they are drawn by a dashed circle. Points A, B, C, D and E are discussed in text.

THEMIS images covers the central south-facing slope of Thaumasia highlands (Fig. 3).

At THEMIS IR scale (Fig. 3), there are many obvious differences in the valley networks than in the visible at Viking scale (Fig. 2). The number of valleys highly increases in comparison to that observed in Viking images. The better spatial resolutions of THEMIS IR images allow us to identify many narrow and shallow secondary tributaries (points A and B in Fig. 3). Moreover, it is apparent now that valley networks dissect the north-eastern-facing slope of Thaumasia highlands (point D in Fig. 3), which was not observed in Viking images (Fig. 2).

Valley networks show a branching-like organisation with a larger tributary at each junction of secondary tributaries. In Warrego Valles, we recognise the major N–S trending, sub-parallel, relatively wide and deep valleys that connect to the main wide, E–W trending tributary that is characterised by segments of straight line arranged at right angles. Many secondary narrow and shallow tributaries developed between them. All valleys are arranged in a hierarchical order (point A in Fig. 3) containing sub-networks as those observed in the northern side of Warrego Valles (at NE of WR in Fig. 3) and in eroded impact craters in the eastern part of the studied area. Note again that the main tributary seems to deepen as it moves down slope.

THEMIS IR images also reveal several valleys on the southern side of the main tributary of Warrego Valles (point C in Figs. 2 and 3). They connect to the main tributary of a large angle, indicating that the local slope is oriented to the north in agreement with the MOLA altimetry. Their spatial organisation is different from that observed in the northern side of the main tributary. They display a sub-dendritic pattern (point C in Fig. 3). A similar valley organisation is also present in the western and southwestern flat areas of Warrego Valles (point E in Fig. 3).

THEMIS images indicate that Warrego Valles developed in a large drainage basin characterised by a concave depression in which a large number of valleys are arranged on both side of the main tributary Valleys on the outside of the drainage basin are arranged in a parallel pattern, whereas valleys in the inner part of drainage basin shows a sub-dendritic pattern. On the northern side of the main tributary, THEMIS images show that the valley heads originate at different elevations from 4 to 8 km, which are higher elevations than previously seen in Viking images (point A in Figs. 2 and 3). On the southern side, valley

heads start at about 4.4 km in elevation (point C in Fig. 3). The location of source areas at different elevations on the both sides of the main tributary of Warrego Valles does not support sapping process, but it would indicate that an atmospheric process combining precipitation and surface runoff was responsible of the difference in elevation of the sources. This interpretation is also supported by the various locations of sources in the secondary valley network on eastern side of Warrego Valles (point B in Fig. 3), valley networks that dissected the northeastern slope of Thaumasia highlands (point D in Fig. 3) and valley heads located at the south of the main tributary of Warrego Valles.

Four separate visible THEMIS images at 17 m/pixel of resolution are used to derive information at the local scale (Fig. 4). Each image was acquired with the 0.654 μm band that is very sensitive to surface albedo (Christensen et al., 2003) and they are located in the central part of Warrego Valles where two types of N–S trending valleys and the main tributary are observed.

The relatively wide and deep valleys are characterised by an opened-V shape and a flat floor (Figs. 4 and 5). They show a relatively constant width of about 700 m (41 pixels) at the top of valleys and 150 m (9 pixels) at the floor. Their maximum depth is around 100 m if we assume a slope in equilibrium of 30° for valley sides. The morphology of the valleys is very smooth. When observed, some valley heads terminate in an amphitheatre shape (Fig. 5) suggesting that they formed by groundwater sapping. No channel has been observed inside valleys, and no outcrop allows us to see the lithology and the geometry of bedrock at this scale. Valleys display a relatively straight path parallel to the slope with a low number of connections before their junction with the main tributary of Warrego Valles. These valleys correspond to the primary channels previously identified on Viking images (Fig. 2). The main tributary of Warrego has

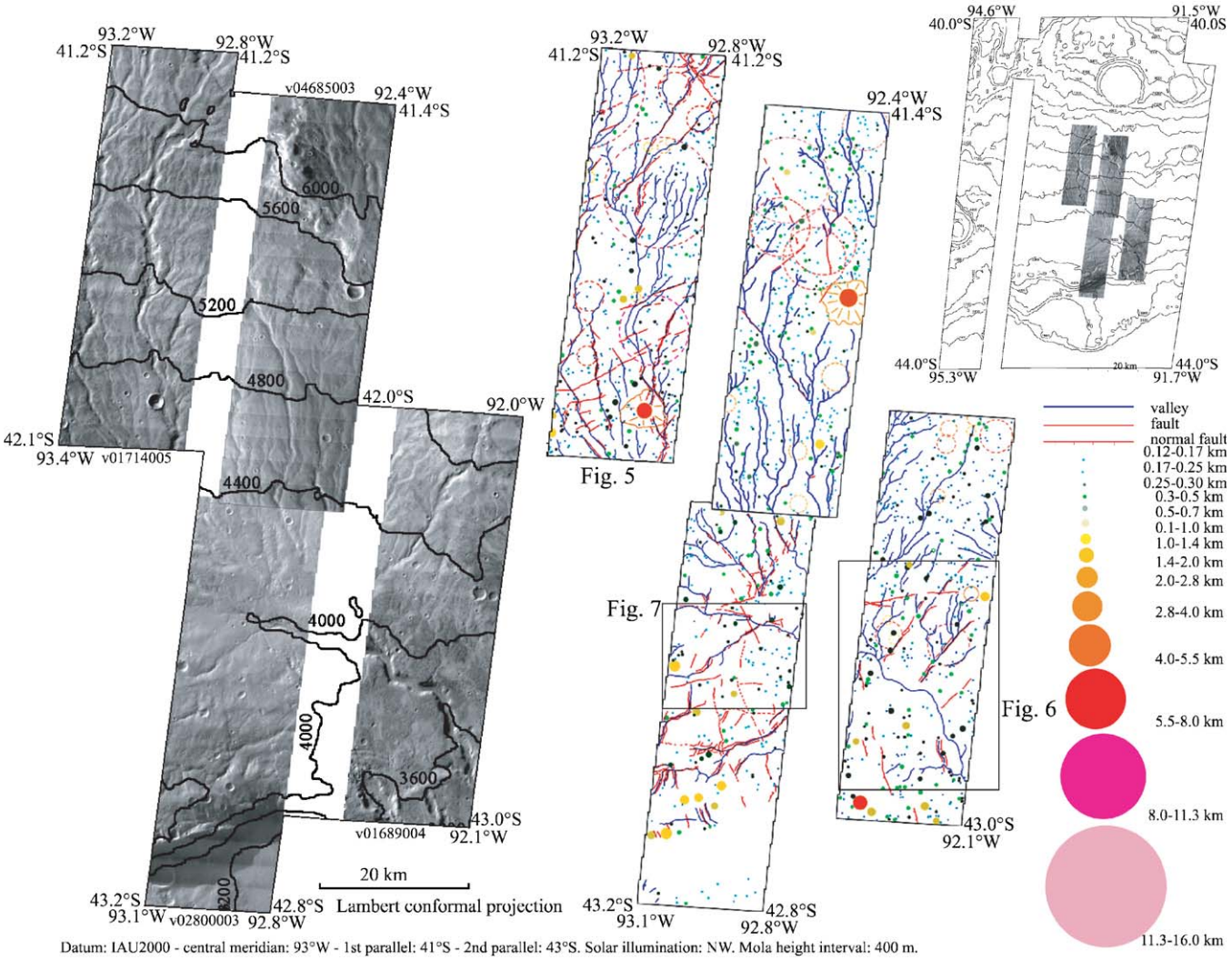


Fig. 4. Mosaic of four visible THEMIS images and its interpretative map. The location of images is given by regional topographic map (on the upper right corner). These high-resolution, visible, THEMIS images (from west to east: V01714005, V04685003, V02800003 and V01689004) have been acquired during afternoon, at ~16 pm, with a resolution of 17 m/pixel and a single band centred at 0.654 μm (band 3). MOLA height contour lines were superposed on visible THEMIS images. We used the same representation of impact crater as that of Fig. 3. Boxes are the location of figure nos. 5, 6 and 7.

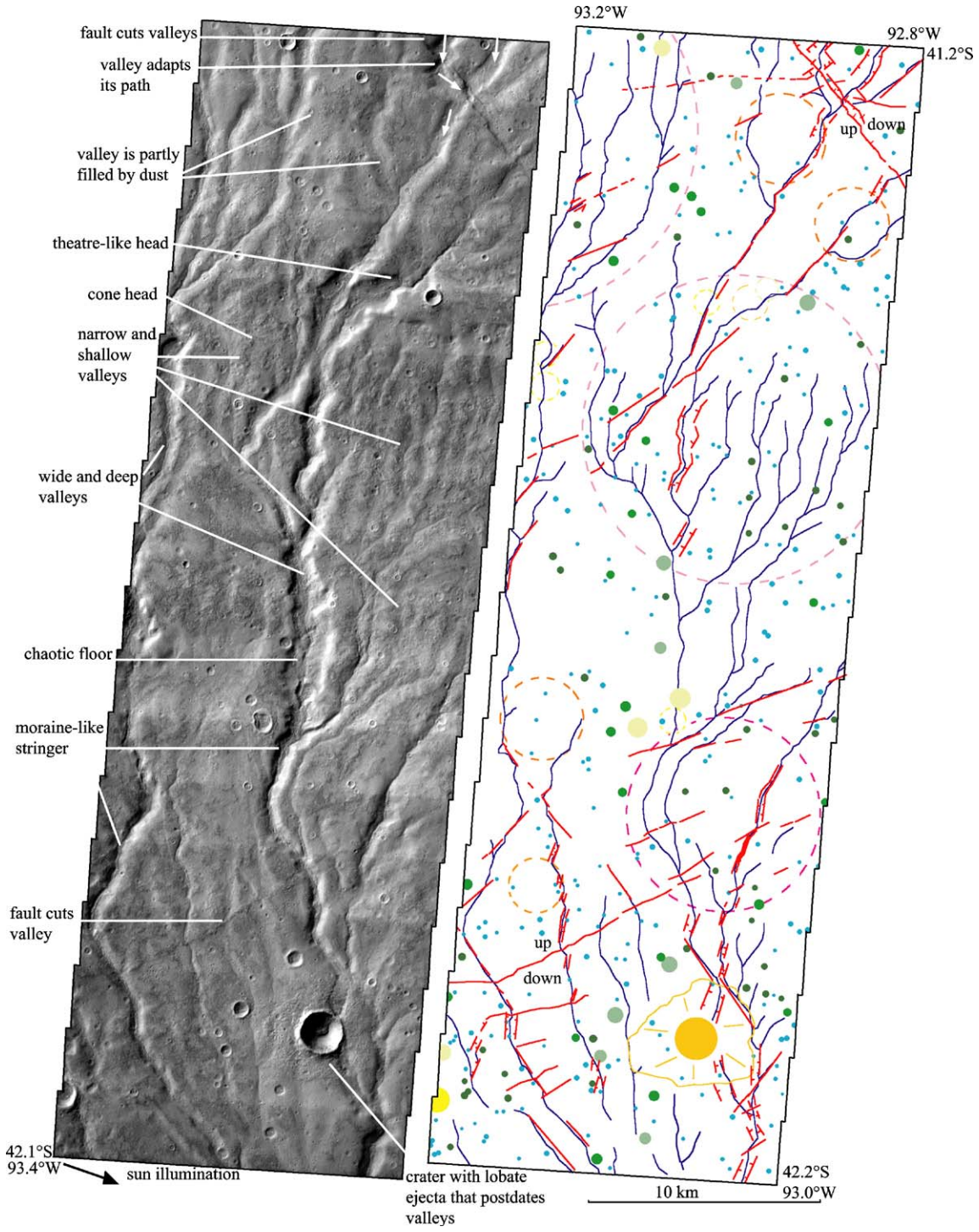


Fig. 5. Visible THEMIS image (V01714005) and its interpretative map. Two kinds of valleys have incised the Warrego Valles: wide and deep valleys, and narrow and shallow valleys. The area is covered by a dust mantle that is crosscut by normal faults. Valleys and intervalleys show a population of small impact craters. Some of them display deformation due to the ice content in the underground.

an opened-U shape. It is ~1400 m wide at the top and ~1000 m wide at the bottom, and it is ~200 m deep at maximum assuming a maximum slope in equilibrium of 30° for valley sides (Figs. 4 and 5).

Narrow and shallow valleys that were not observed on Viking images are observed both in THEMIS IR and visible images (Figs. 3 and 4). Typically, these valleys are located between the major N–S trending wide valleys. Their distribution is ubiquitous, and their number is often high (Fig. 5). In the THEMIS visible images, their geometry is characterised by a $<250$ m wide (14 pixels) and $<50$ m deep, V-shape. They show a branching-like pattern before their connection to the wide and deep valleys. Locally, their heads are characterised by a small

conic shape (Fig. 5) standing at different elevations, suggesting that they formed by surface runoff.

### 2.2. Tectonic modifications of valley networks

The region of Thaumasia highlands is characterised by a large number of tectonic structures including folds and faults identified from Viking mosaics (Tanaka et al., 1998; Dohm and Tanaka, 1999; Dohm et al., 2001). Warrego Valles is cut by three networks of grabens (Figs. 2 and 3). In THEMIS images, many valleys display a straight path bounded by one of the 1 km long faults (Figs. 5 and 6), indicating that the arrangement of valleys is highly controlled by tectonics. The northwestern part of Warrego Valles is controlled by networks of NNE–SSW and NNW–SSE trending normal faults (Figs. 3 and 4). Some pristine valleys could have been widen by the faults. Faulting may have also affected the main tributary of Warrego Valles because its path is at right angle, which is suggestive of tectonic control (Figs. 4 and 6).

Fault movement appears to have occurred at the same time as valley formation (Figs. 5 and 6). For example, NNW–SSE trending normal faults cut two valleys that flowed to the southeast (upper right corner of Fig. 5). As the southern block was lifted, water could not flow downstream. As a result, the water flow deviated from its path, incised the fault scarp and captured another valley downstream (Fig. 5). In addition, some valleys are perched (Fig. 6) indicating that valleys have been lifted by tectonics preventing water to flow inside them. Several valleys are also cut by normal faults without late incision indicating that valley formation stopped when they were displaced by faulting (Fig. 5).

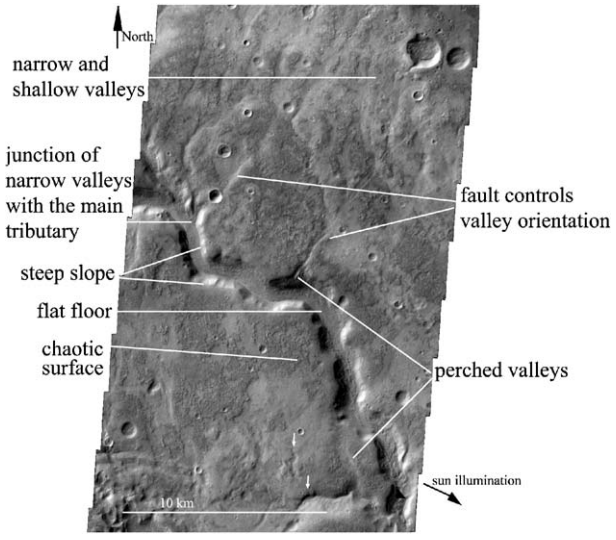


Fig. 6. Extract of visible THEMIS image (V01689004). The main tributary of Warrego Valles shows a steep side and flat floor with a chaotic surface. Secondary valleys connect to the main tributary. The orientation of these valleys is highly controlled by fault tectonics. Note perched valleys in different parts of image.

### 2.3. Morphologic modifications of valley networks

Both THEMIS visible and high-resolution MOC images revealed that the valleys were degraded by depositional and erosional processes following their formation (Malin et al., 1998; Carr and Malin, 2000). In THEMIS visible images, the relative wide and deep valleys display a smooth surface suggesting that they have been partially filled or mantled by homogeneous and fine-grained material (Figs. 4 and 5). The pristine morphology of narrow and shallow valleys is also masked by a dust mantle. Note that there is a lower number of valleys on the southern side of Warrego Valles (Figs. 4 and 7) than on the northern side, which could be due to the relatively thick mantle of dust in this location.

In the 22 high-resolution MOC images available in the Warrego Valles (Fig. 8a), valley and intervalleys are covered by a dust mantle (Fig. 8b–f). The thickness of the dust mantle seems to be deep in several areas. In the southern part of Warrego Valles, late erosion allowed us to estimate the minimum thickness of dust mantle and its geometry. An outcrop ~140 m (26 pixels of 5.55 m in width) high exhibits many superposed dark and bright sub-horizontal layers (Fig. 8d) suggesting a cyclic process deposited the dust.

Although the surface of dust mantle appears relatively smooth at the resolution of THEMIS visible images, it appears relatively rough at the MOC scale, with a chaotic pattern of pits and mottles (Fig. 8c–f). This surface pattern could be created if ice was contained in the dust mantle and later sublimed. Indeed, the studied area is located at 40°S of latitude where this kind of surface morphology is common and interpreted as water–ice-rich deposits (Squyres, 1989; Squyres et al., 1992; Mustard et al., 2001; Mangold, 2003; Head et al., 2003). Within relatively wide and deep valleys, the dust mantle displays not only the chaotic pattern but also longitudinal convex-up features that resemble longitudinal moraines (Fig. 8e). This suggests that the ice content may be sufficiently high to induce ice creep or ice flow. In addition, valley sides show mass

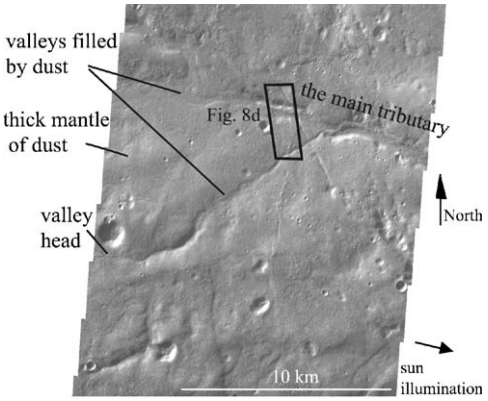


Fig. 7. Extract of visible THEMIS image (V02800003). Valleys are often filled by dust material that exhibits a smooth texture at THEMIS visible scale. Note the partially buried or filled craters. See text for explanation. The black box corresponds to Fig. 8d.

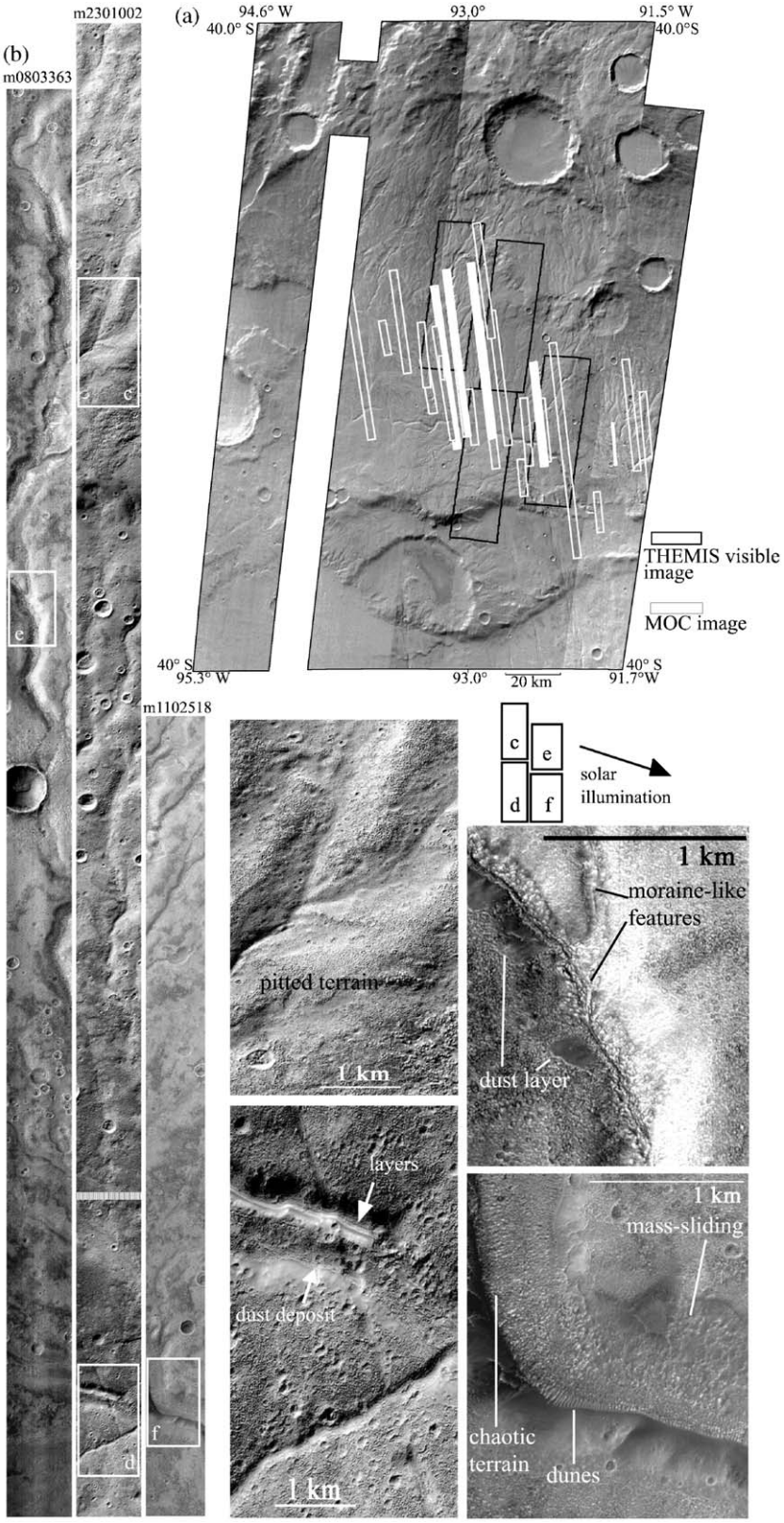


Fig. 8. (a) Location of visible THEMIS and 22 MOC images available in the Warrego Valles. Each MOC image covers an area of ~3 km in width × ~80 km in length with a nearly north–south trending with a resolution ranging from 1.5 to 5.5 m/pixel. The filled white box corresponds to the location of three MOC images seen at the right part of the figure. (b) MOC images with degraded resolution. Extracts of MOC images with better resolution: (c) dust mantle within valleys and pitted terrains; (d) geometry of dust mantle (layered) in the main tributary of Warrego Valles; (e) chaotic or pitted surface of mantle and moraine-like features within filled valleys and thin, smooth dust cover on valley sides; (f) the main tributary of Warrego Valles near its mouth with its steep side covered by smooth, thin dust and flat floor locally covered by aeolian dunes.

movements or "debris flows" (Fig. 8f), which suggests that this material could contain ice that enables it to move slowly down.

A thin, smooth, fine-grained dust layer (volcanic or aeolian nature) systematically covers the north-facing and east-facing slopes of wide and deep valleys (Fig. 8c, e and f). This thin layer of dust seems to be relatively recent because of the lack of impact craters. Notice that small aeolian dunes are observed at the toe of north-facing slope of the main tributary of Warrego Valles (Fig. 8f), which indicates that fine particles (<2 mm) are recently transported by wind within this valley.

### 2.4. Impact craters and chronology of events

Thaumasia highlands show numerous, <100 km in diameter impact craters, with eroded rims and flat floors (Fig. 2). Such craters may have been modified as the valley networks forming during the Noachian (Craddock and Maxwell, 1990, 1993). These impact craters are often deformed by tectonics, such as the one situated on the southern boundary of Thaumasia highlands (Fig. 2, 93.5°W–43.5°S). Sometimes they are filled by material, such as one located at 95.2°W–42.5°S (Fig. 2). This suggests that they were modified by weathering, or they may be partially filled by mass wasting, aeolian or lacustrine deposits. In THEMIS IR images, these craters exhibit an internal rim eroded by short, straight gullies, e.g. crater located at the top of the Thaumasia highlands (Fig. 3, 92.5°W–40.5°S).

Different stages of degradation are observed for small (<3 km in diameter) craters (Fig. 9) in visible THEMIS and MOC images. The initial stage displays a bowl shape surrounded by ejecta (Fig. 9a and b) (Strom et al., 1992). For craters greater than 2 km in diameter, the ejecta is lobate suggesting that ice or water was contained in the ground when the impact occurred (Fig. 9a and b) (Strom et al., 1992). More heavily modified craters are irregular in shape with collapsed interiors (Fig. 9c and d) and infilling by dust. Their shape could result from the viscous relaxation due to ice content, which occurs in the areas located below 40°S (Squyres, 1989; Squyres et al., 1992; Mangold, 2003). An advanced stage of modification is characterised by rimless craters which are almost completely filled by aeolian dust (Fig. 9d and e). The final stage of modification corresponds to "ghost" or highly degraded craters, which is the circular shape remaining (Fig. 9e and f) after intense erosion and infilling. These different stages of crater modification suggest again that Warrego Valles was subjected to intense depositional and erosional processes (Hartmann and Esquerdo, 1999). However, a small population of impact craters showing the initial morphology is observed whatever the image resolution. In THEMIS visible images, these impact craters are often <8 km in diameter, whereas they appear to be more numerous in MOC images, with diameters ranging from 8 to 0.3 km.

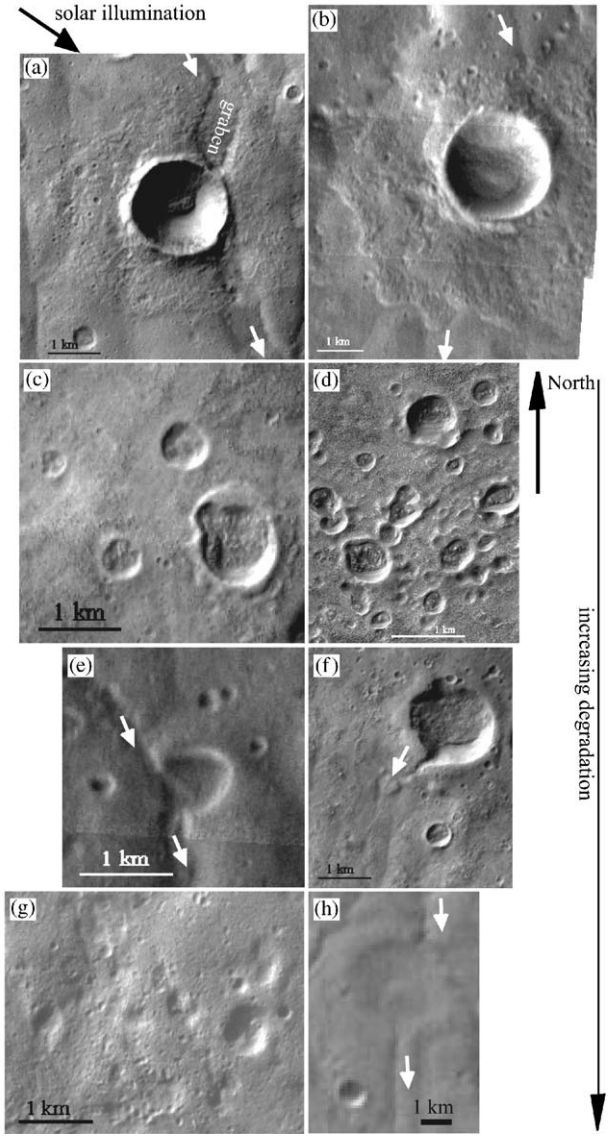


Fig. 9. Different stages of modification observed in impact craters. These examples are extracted from visible THEMIS and MOC images.

The spatial distribution of impact craters is locally heterogeneous, but we suspect that it is a consequence of external processes rather than a reflection of the age of the terrain. Impact craters are more numerous on the northern side of the main tributary of Warrego Valles than on the southern side, which can be explained by the thick dust mantle present on the latter (Fig. 3, 4 and 7). The minimum size of impact craters observed in areas covered by dust mantle is 0.4 km, which corresponds to the mean diameter of highly degraded or buried craters. Based on this mean diameter, the thickness of dust mantle is estimated at least ~50 m in average using models of filling of craters (Garvin et al., 2002; Vincendon et al., 2002). The largest highly modified crater observed in Warrego Valles is 2.8 km in diameter (Fig. 9f), which implies the dust mantle is at least 150 m thick at this location. This is consistent with the apparent thickness of layered dust mantle of ~140 m

observed on the southern side of main tributary of Warrego Valles in MOC image (Fig. 8d).

A relative chronology of valley formation was established by crosscutting relationships with impact craters. Large craters are usually incised by valleys (Fig. 2, 3 and 4) indicating they formed before valleys. Some small craters are also incised by valleys (Fig. 9e and f) suggesting that valleys formed after these craters. It is probable that these small impact craters formed in the late stage of Warrego Valles formation because of their relative preservation. Numerous small impact craters have impacted the valley networks, and thus post-date valley formation (Fig. 9a, b and h). Thus, we discriminate two populations: craters formed before or during valley network formation (ante craters) and those that post-date valley network formation (post-craters). The end of valley formation can be estimated from the post-craters using standard cratering counting techniques applied to the entire Warrego Valles drainage basin. We performed cumulative crater counts per $10^6\,km^2$, for craters greater than 5 and 2 km in diameter (N[5] and N[2]) for the both populations of impact craters (ante and post). The numbers of the total crater population are (~1000 for N[2] and ~450 for N[5] (Table 1), suggesting that the bedrock of Warrego Valles dated from the Noachian to the early Hesperian (Tanaka, 1986). The age of the end of valley formation can only be estimated from the N[2] cumulative count (~750, Table 1), owing to the lack of craters greater than 2 km in diameter within the drainage basin. The valley formation seems to have stopped by the late Hesperian. These two ages are consistent with those associated to the (HNpld) geologic unit of intermediate dissected material, i.e. >700 for N[2] and >100 for N[5] (Dohm and Tanaka,1999; Dohm et al., 2001).

The distribution of craters per square kilometre versus their diameter (Fig. 10) can be plotted in a logarithmic incremental histogram (Hartmann and Neukum, 2001) for both Viking and THEMIS images excepted MOC images. This method uses a theoretical crater distribution curves for a period of time that correspond to "isochrons", i.e. the crater distribution per square kilometre expected for a Martian terrain not modified by surface processes. The total population of craters ranges from 150 m to 16 km in diameter depending on the imagery data. The craters formed before valleys date to the Noachian, even their distribution is not significant for the largest craters because of their low number relative to the small surface covered by the drainage basin. The craters formed after valleys date from the middle to late Hesperian for diameter classes greater than 400 m. The classes of smaller craters (<400 m) crosscut isochrons younger than 3 Gyr, which indicates the impact cratering rate has not been sustained in comparison to external geologic processes (resurfacing), since 3 Gyr (late Hesperian). Warrego Valles formed during an interval of time between 3.5 and 3.0 Gyr but it is difficult to establish its real duration of formation by the crater counting method alone.

In summary, the THEMIS IR images provide a significant advance in understanding the complexity of Warrego Valles, revealing valleys partly buried under dust. High-resolution images from THEMIS visible to MOC allow us to study the morphology of valleys and place their modifications in recent context. By analysing all the available data, we can conclude that: (1) the valley networks of Warrego Valles are not isolated on the southern side of the Thaumasia highlands as previously reported; (2) it developed in a rectangular-shaped, concave-up drainage basin with an increasing number of valleys on both sides of the main tributary; (3) valleys are organised in Earth-like, branching fluvial networks, with sub-networks controlled by topography inherited from impact craters; (4) the valley pattern seems to be highly controlled by tectonics and topographic slope (parallel pattern on the northern side and dendritic pattern on the central flat part of Warrego Valles); (5) valley heads are located at different elevations, which is consistent with an atmospheric water

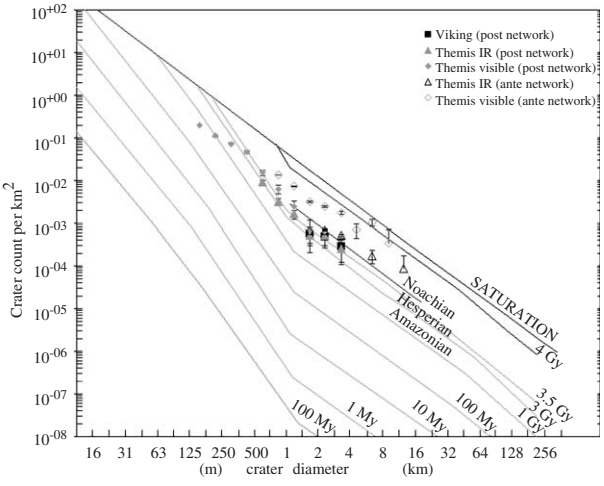


Fig. 10. Distribution of impact crater per square kilometre versus diameter. Isochron lines correspond to Hartmann and Neukum's (2001) curves.

Table 1
Cumulative crater count and age of Warrego Valles

| | Post-valley N(2) | Network N(5) | Epoque | Ante valley N(2) | Network N(5) | Epoque |
|---|---|---|---|---|---|---|
| Viking (230 m/pixel) | 764±27 | — | Hesperian | 955±30 | 191±13 | Hesperian inf. |
| THEMIS IR (101 m/pixel) | 776±27 | — | Inf. | 1552±39 | 689±26 | Noachian |
| THEMIS visible (17 m/pixel) | 697±26 | — | Hesperian sup. | — | — | |

cycle; (6) valley networks were formed since the Noachian and stopped in the late Hesperian, i.e. ~3 Gyr ago; (7) valleys have then undergone modifications (impact cratering, mass-sliding, dust blurring and filling, ice deformation, etc.) since their formation.

## 3. Morphometry of Warrego Valles

We analysed the morphometry of Warrego Valles by using both the imagery at different scales and the MOLA altimetry. The latter allowed us to quantify different parameters as height difference, topographic slope, etc. at a spatial resolution of ~500 m.

### 3.1. Warrego Valles from MOLA altimetry

We generated a digital elevation model (DEM) representing the topography of Warrego Valles (Fig. 11) based on MOLA data interpolated with a spatial resolution of 128 pixels/degree or ~463 m/pixel (Smith et al., 1999, 2001). Numerous, <100 km in diameter impact craters, NNW–SSE narrow grabens, and NNE–SSW trending, normal faults bounding rift valley (NW corner in Fig. 11) can be seen in the resulting DEM. The valley network of Warrego Valles is nearly invisible. The eastern outlet of the main tributary is just visible, indicating that the valley network is shallow at MOLA resolution.

We used a hydrologic analysis (DNR hydromod) included in ARCVIEW GIS (Loesch, 2001) in order to extract the valley networks from the DEM. The program consists of three steps: (1) the original topography (DEM) is modified removing sinks to produce a continuous flow direction grid. This step is very important because sinks (such as pits or impact craters) can disrupt the drainage topography; (2) a flow direction grid is calculated from the centre of cell to the steepest down-slope direction of the eight neighbouring cells (D8 algorithm); (3) an accumulation flow grid is generated as the cumulative number of cells flowing into each down-slope cell. Cells that have high accumulation may be used to identify stream channels or valleys.

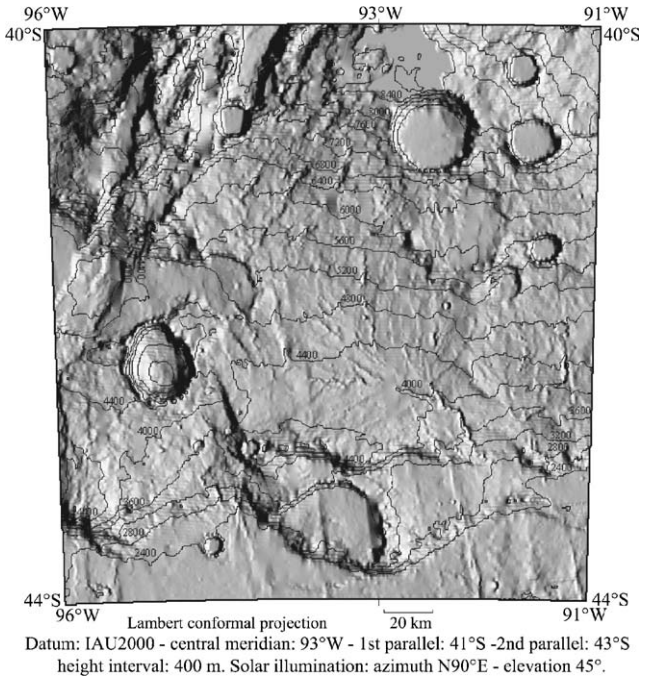


Fig. 11. Shaded topographic map of Warrego Valles based on MOLA data. Despite the incidence angle of illumination, the valley network of Warrego Valles is lowly sighted. Only the last 50 km near the mouth is obviously emphasised by sun illumination owing to the large incision in this area.

In the studied area, numerous valley networks are detected (Fig. 12a). The valley networks are distributed in a divergent pattern around the summit of the Thaumasia highlands. Warrego Valles is characterised by a low number of valleys distributed in three sub-networks located on the northern side of the main tributary. Valleys are parallel, N–S trending with few branches. The valley trending seems to be controlled by topographic slope and tectonic features (Figs. 11 and 12a). Notice that several valleys are detected on the southern side of the main tributary. They display few branches, and they connect directly to the main tributary of Warrego Valles which the outlet is far east dissecting the Sirenum plain.

### 3.2. Geometric properties of valley networks at different scales

Valley networks have quantifiable sets of geometric properties (Strahler, 1968). Our study has increased the total number of valleys including 45 valleys detected with MOLA data, 262 valleys with Viking images at 1:560,000 scale and 1027 valleys with IR THEMIS images (Table 2 and Fig. 12). The total number of valleys increases about four times between each data set whereas the spatial resolution increases twice, e.g. MOLA (463 m/pixel), Viking (230 m/pixel) and IR THEMIS (101 m/pixel) images, respectively. The total length of valleys also increases twice between each data set (Table 2): 1350.850, 2880.820 and 6161.040 km for MOLA, Viking and THEMIS IR images, respectively. Note that only 48 valleys had been previously counted from Viking Orbiter photomosaic at a scale of 1:2 million (Cabrol and Grin, 2001). The total length of Warrego Valles is also different from the previous calculation based from Viking, e.g. 860 km (Cabrol and Grin, 2001).

### 3.3. Geometric relationships with valley order

We analysed the drainage composition of Warrego Valles in which the relationship between different magnitude of valleys or "streams" can be expressed in mathematical terms (Horton, 1945). Indeed, a terrestrial valley network is distinguished by a great number of valleys in which stream flow is arranged in branch-like pattern that diminish in size away from the main tributary. Each valley

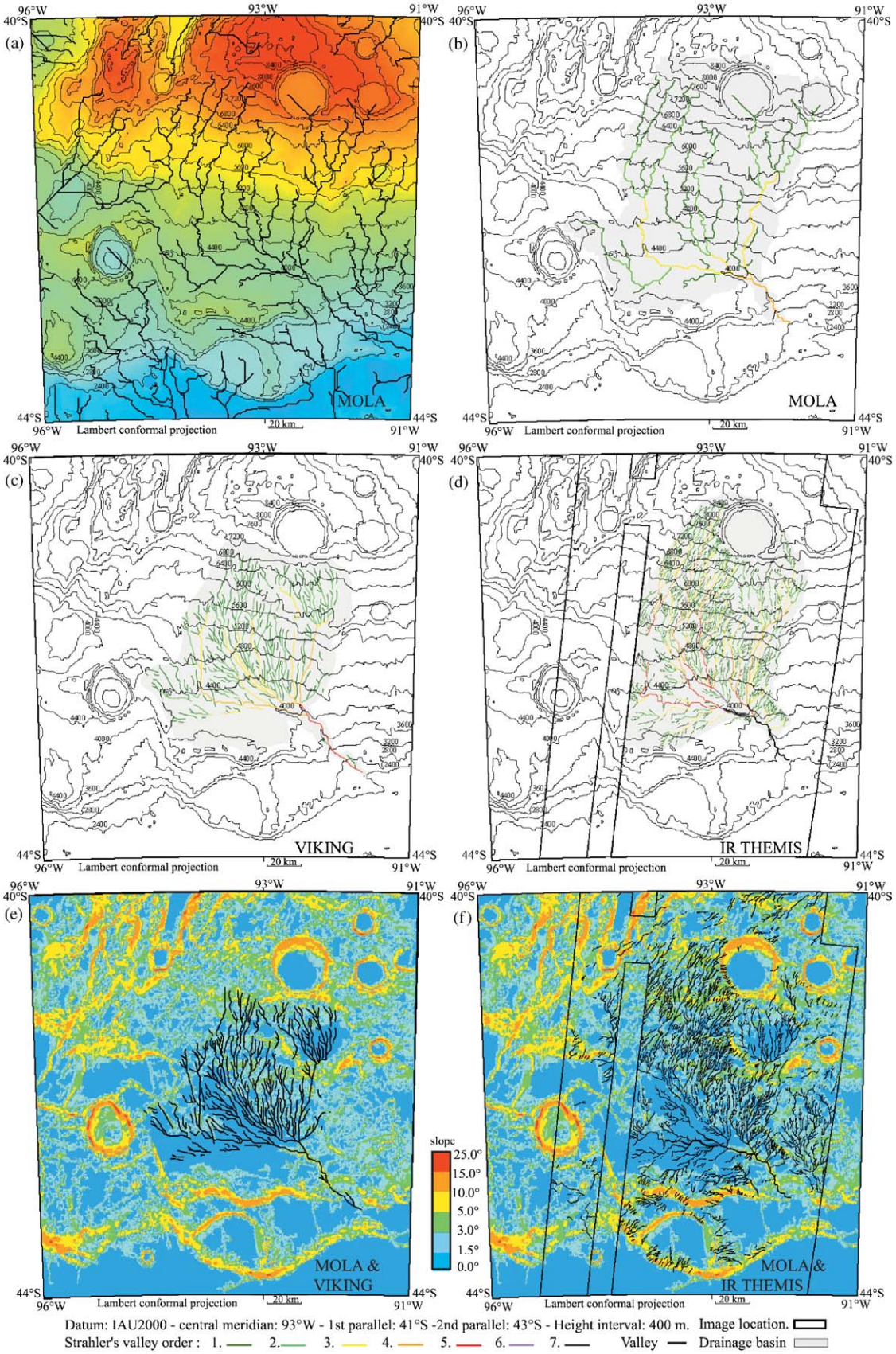


Fig. 12. (a) MOLA topographic map with contour lines spaced of 400 m. Valley networks automatically detected are plotted. Warrego basin and Strahler's orders are mapped from (b) MOLA data, (c) Viking image and (d) IR THEMIS images. Patterns of valley network versus local topographic slopes from (e) Viking and (f) IR THEMIS images.

Table 2
Topology of Warrego Valles

| | MOLA (463 m/pixel) | Viking (230 m/pixel) | THEMIS IR (101 m/pixel) |
|---|---|---|---|
| Maximum order of valleys | 4 | 5 | 7 |
| *Order 1* | | | |
| Number of valleys | 32 | 199 | 745 |
| Mean length (km) | 21.664 | 7.480 | 3.79 |
| Median length (km) | 17.504 | 6.250 | 2.73 |
| Maximum length (km) | 693.250 | 1488.900 | 2822.20 |
| *Order 2* | | | |
| Number of valleys | 9 | 42 | 202 |
| Mean length (km) | 44.232 | 16.990 | 8.21 |
| Median length (km) | 52.730 | 15.750 | 6.26 |
| Maximum length (km) | 398.090 | 764.680 | 1658.19 |
| *Order 3* | | | |
| Number of valleys | 3 | 16 | 57 |
| Mean length (km) | 66.842 | 23.370 | 15.57 |
| Median length (km) | 82.450 | 10.750 | 10.94 |
| Maximum length (km) | 200.530 | 373.960 | 887.28 |
| *Order 4* | | | |
| Number of valleys | 1 | 4 | 15 |
| Mean length (km) | — | 44.580 | 28.40 |
| Median length (km) | — | 39.680 | 22.51 |
| Maximum length (km) | 58.97 | 178.33 | 425.98 |
| *Order 5* | | | |
| Number of valleys | — | 1 | 5 |
| Mean length (km) | — | — | 54.25 |
| Median length (km) | — | — | 39.16 |
| Maximum length (km) | — | 74.950 | 271.24 |
| *Order 6* | | | |
| Number of valleys | — | 1 | 2 |
| Mean length (km) | — | — | 13.32 |
| Median length (km) | — | — | 13.32 |
| Maximum length (km) | — | 74.950 | 26.64 |
| *Order 7* | | | |
| Number of valleys | — | — | 1 |
| Mean length (km) | — | — | — |
| Median length (km) | — | — | — |
| Maximum length (km) | — | — | 69.50 |
| Total number of valleys | 45 | 262 | 1027 |
| Total length (km) | 1350.850 | 2880.820 | 6161.040 |
| Bifurcation number ($R_b$) | 3.1 | 3.7 | 2.8 |
| Valley length number ($R_l$) | 1.5 | 1.8 | 1.7 |
| Drainage area ($km^2$) | 14,254.590 | 10,462.320 | 11,596.000 |
| Drainage density ($km^{-1}$) | 0.09 | 0.27 | 0.53 |

thus corresponds to a segment of the valley network. Such valleys are assigned an order indicating its relative importance in the network. In the Strahler' (1952a) system, the lowest order is a segment with no tributary and is designated as a first-order valley. Where two segments of first order join together, they form a second-order segment and so on. Where two segments of different orders join together, the following segment retains the highest order. The highest order of valley network corresponds to that of the main tributary (outlet).

As Strahler's method is based on the recognition of first-order valleys, it is highly dependent on the scale of data (Table 2). At 1:2,000,000 Viking scale, three orders were found (Cabrol and Grin, 2001). With MOLA data, Warrego Valles is characterised by a magnitude of four orders (Fig. 12b), and the magnitude of valleys increases with the data resolution, so that we observe five and seven orders for Viking and THEMIS IR images, respectively (Fig. 12c and d). The high magnitude of valleys found in THEMIS IR images can be explained by the detection of small valleys partially filled with dust owing to variations of thermal properties of materials. The original magnitude could nevertheless be underestimated because of 3 Gyr of dust infilling and/or erosional processes.

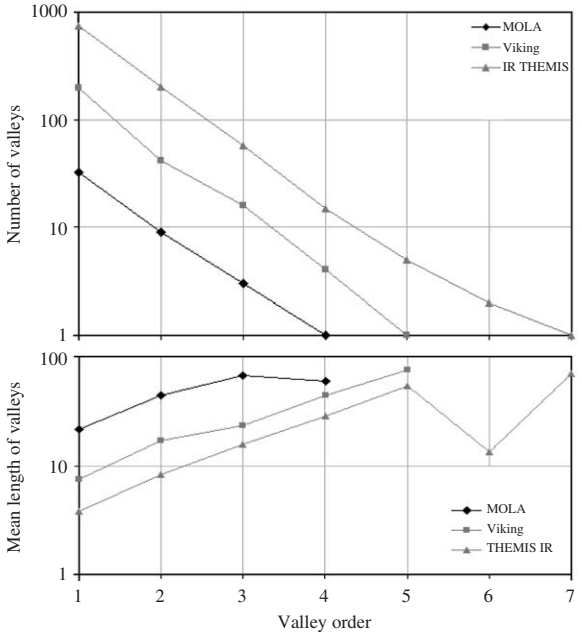


Fig. 13. Number of valleys and mean length of valley versus valley order for network of Warrego Valles mapped from MOLA data, Viking and IR THEMIS images.

The linear relationships between valley order and the number of valleys associated to a given order have been presented in a semi-logarithmic graph (Schumm, 1956). For Warrego Valles, valley numbers of different orders follow the same linear law versus their respective order whatever the data set (Fig. 13).

The bifurcation ratio ($R_b$) is defined as the ratio of the number of valleys for a given order ($N_u$) to the number of valleys in the next higher order ($N_{u+1}$). Although the bifurcation ratio is not constant from one order to a higher one, its variation is very low. The mean value ($R_b$) is ~3 for Warrego Valles whatever the data set (Table 2). The average valley length also follows a linear function with the respective valley order for most terrestrial valley networks (Schumm, 1956; Strahler, 1968). For Warrego Valles, this relationship is confirmed (Fig. 13): higher-order valleys are also longer valleys. For minor tributaries, the average length is less than ~20 km, whereas the main tributary is ~65 km long (Table 2). Note that the sixth-order valley identified in THEMIS IR images shows a drop in length due to the lack of valley continuity buried under dust (Fig. 13). The length ratio ($R_l$) is the ratio between the average length of valley of a given order ($L_u$) to that of the next higher order ($L_{u+1}$) (Horton, 1945; Strahler, 1952a, b). For each Martian data set, the $R_l$ value is close to 1.7 (Table 2).

The morphometric parameters of Warrego Valles such as valley order, bifurcation ratio and valley length ratio give values similar to terrestrial valley networks. Indeed, the terrestrial $R_b$ values ranges from 3.0 to 5.0 (Horton, 1945) and the terrestrial $R_l$ value ranges from 1.5 to 3.5 (Horton, 1945; Strahler, 1968; Ritter et al., 2002). We can compare the morphometric parameters of Warrego Valles to those of Kohala volcano in Hawaii that exhibits a style of fluvial dissection similar to Warrego Valles (Table 3). In the southwestern part of Kohala volcano, valley networks have eroded ash deposits 0.4 Myr old (Gulick, 1987, 2004). They show a low magnitude (<4 Strahler's orders) with a bifurcation ratio of 2.9 and a length ratio of 2.1 (Table 3). These values are close to those of Warrego Valles. Nevertheless, these parameters are empirical and their meanings in terms of physical processes remain unclear on Earth.

Table 3
Morphometric parameters of Warrego Valles compared to those of the SW part of Kohala volcano (Hawaii) in semi-arid climate regime

| | Warrego Valles | Kohala volcano |
|---|---|---|
| Bifurcation number ($R_b$) | 2.8 | <2.9 |
| Valley length number ($R_l$) | 1.7 | <2.1 |
| Drainage density ($km^{-1}$) | 0.53 | 0.3–1.1 |
| Relief ratio (deg.) | 1.4 | 7.6 |
| Network pattern | Dendritic–sub-parallel | Sub-parallel |
| Ruggedness number | 3.3 | 0.5–2.1 |
| Lithology | ? | Ash deposit |
| Age | 3 Gyr | 0.4 Myr |

For Warrego Valles, values correspond to those extracted from THEMIS IR images (101 m/pixel) at ~1:142,000 scale. For Kohala volcano, values are extracted from different works (Gulick, 1987, 2004) and partially calculated from the map of fluvial valleys on Kohala volcano at 1:250,000 scale (Gulick, 2001).

### 3.4. Valley pattern in relation with topographic slope

On Earth, drainage pattern depends on the slope of the basin (Phillips and Schumm, 1987; Schumm et al., 1987). The relief ratio is defined as the ratio between the difference in elevations of the basin to the maximum horizontal length along the main tributary. It corresponds to a slope of 2.4% or 1.4° for Warrego Valles. On low slopes, drainage networks formed by rainfalls exhibit a dendritic pattern with a strong correlation to junction angle for the first-order tributaries (Phillips and Schumm, 1987; Schumm et al., 1987). Empirical data show a dendritic pattern develops on a slope lower than 1% with a minimum junction angle of 60° and reaching 90° on flat terrain. A sub-parallel pattern develops on slope >3% with a junction angle of about 40° in a homogeneous sandy materials without tectonic control.

Warrego valley network displays a similar pattern in relation with local slope (Fig. 13d and e): the south-facing slope of Warrego Valles displays a sub-parallel pattern with a junction angle lower than 34° whereas the central flat depression shows a dendritic pattern with a junction angle of 54° for the principal tributaries. This correlation would be consistent with a fluvial origin involving runoff process.

### 3.5. Drainage density

The drainage basin is defined as the area in which water and sediments are collected and distributed, bounded by the highest topographic points. The boundary of a drainage basin within an image is usually difficult to determine because it is defined by topography which can often be subtle. We thus adapted a methodology used by several investigators (Kochel, 1985; Baker and Partridge, 1986) by superposing MOLA topographic data on imagery data. This results in different sizes of the drainage basins according to data set (Fig. 12). The drainage basin of Warrego Valles covers an area of 14,255 $km^2$ based on the THEMIS IR data (Table 2).

Drainage density ($km^{-1}$) is the sum of the length (km) of all individual valleys inside the drainage basin divided by the total area of the drainage basin ($km^2$) (Table 2). We found a drainage density of 0.53 $km^{-1}$ using THEMIS IR images, which is orders of magnitude larger than those found (0.005–0.15 $km^{-1}$) in previous studies of valley networks formed in densely cratered uplands (Baker and Partridge, 1986; Carr, 1995, 1996; Carr and Chuang, 1997; Grant, 2000). The drainage density of Warrego Valles is twice what was calculated from Viking images, i.e. 0.27 $km^{-1}$ (our study) and 0.21 $km^{-1}$ (Cabrol and Grin, 2001), and it is nearly six times higher than the value calculated from MOLA data, i.e. 0.09 $km^{-1}$ (our study) and 0.06–0.11 $km^{-1}$ for valley networks located in dissected Noachian terrains (Stepinski and Collier, 2003). Obviously, drainage density is highly dependent on the map scale (Carr, 1995). The scale of THEMIS IR images is equal to 1:142,000 and approaches the scale used for mapping terrestrial drainage systems, which ranges from 2 to 30 $km^{-1}$ (Carr, 1995). However, if we compare the drainage density of Warrego Valles to that obtained on Kohala volcano in Hawaii at a scale twice smaller (Table 3). We note that Warrego Valles displays the same magnitude as valley networks incising the Hawaiian volcano, e.g. 0.3–1.1 $km^{-1}$ (Gulick, 1987, 2001, 2004; Gulick and Baker, 1990).

On Earth, the drainage density reflects the spacing of the tributaries and the interaction between climate and geology. On the one hand, it is widely related to precipitation (rate and intensity), and it is used to predict runoff properties at macro-scale (Morgan, 1973; Gregory, 1976; Abrahams, 1972, 1984). In terrestrial desert climates, the drainage density is usually low when the precipitation intensity is high. For example, the drainage density is $<9\,km^{-1}$ when the precipitation intensity is $>50$ mm/24 h in the USA (Abrahams and Ponczynski, 1984). The result of this climatic phenomena is well expressed on Hawaiian volcanoes as the valley networks of the southwestern side of Kohala volcano have formed in semi-arid climatic regime (Gulick, 2001). By comparison, the low drainage density of Warrego Valles could be explained by climatic conditions in which precipitation occurred intensively and episodically such as seen in a desert or semi-arid climate on Earth.

Additionally, drainage density also depends on the lithology (soil), the resistance of surface material to the erosion and the infiltration capacity of material (soil). For small terrestrial basins, infiltration capacity is the main factor controlling drainage density (Carlston, 1963). For example, an unvegetated surface consisting of resistant material with a high permeability usually exhibits a network with widely spaced valleys, yielding a low drainage density (Patton and Baker, 1976; Ritter et al., 2002). In Hawaii, the low drainage density is associated with ash deposits and soil horizons characterised by an average permeability (Gulick and Baker, 1990; Gulick, 2001, 2004). On Mars, if drainage density is controlled by lithology, we infer that the ground was resistant to erosion and possessed a high permeability when the valleys formed. However, the geology of the substratum of Warrego Valles is unknown at present because the surface is characterised by dissected and etched material consisting of alluvial and colluvial deposits mixed with older volcanic rocks at the Viking scale (Dohm et al., 2001). The substratum of Warrego probably consists of regolith, impact debris and volcanic material, as the area has been intensively cratered. In such a case, it could be characterised by a high permeability, and thus a less developed network at the surface.

There is a high correlation between basin area and peak flow discharge on Earth. The ruggedness number (Melton, 1958) which is defined as the product of basin relief and drainage density, could be used to predict the flash flood potential. If we assume that this relationship between precipitation and basin area can be applied on Mars, the ruggedness number of Warrego Valles is 3.3, which is comparable to terrestrial values in Utah, South California and West Texas (Ritter et al., 2002) independent of the lithology. Warrego Valles should be characterised by a high flash flood potential because of the high ruggedness number (Patton and Baker, 1976). In addition, the ruggedness number of Warrego Valles would relate to semi-arid to arid climate on the Earth.

### 3.6. Basin stage in Davis' geomorphology

The drainage density of natural streams increases with time in order to reach an equilibrium with climate and geology (Schumm, 1956). The elevation-basin area hypsometric curve can be used to analyse the erosional topography of drainage basin and determine the qualitative stage of drainage basin development in Davis' geomorphic cycle. Strahler (1952b) defined the hypsometric curve with normalised parameters as the ratio of the elevation difference between a given point and the basin mouth to the basin height difference versus the ratio of area above the elevation of given point to the basin area. The smooth S-shaped curve crossing the centre of diagram indicates that Warrego Valles has reached the equilibrium stage or maturity (Fig. 14). The mean altitude of Warrego Valles is 5567 m and the mid-area of the drainage basin stands $>5400$ m in elevation, which suggests that the basin has a

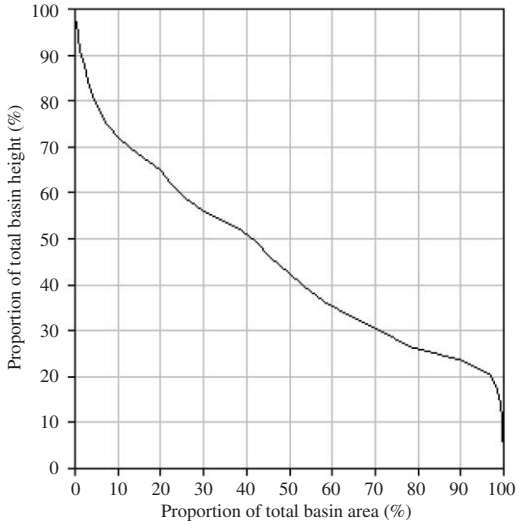


Fig. 14. Hypsometric curve derived for Warrego Valles from MOLA data. The hypsometric integral is equal to 0.46.

nearly regular topographic slope. In addition, the hypsometric integral, defined as the volume of rocks resistant to the erosion (area below the hypsometric curve), provides a measure of the dissection of landscape. The hypsometric integral of Warrego Valles is equal to 0.46, which is in agreement with the Davis' maturity stage in which denudational and slope processes are in balance.

On Earth, the hypsometric curves and integrals have been interpreted in different ways taking into account the basin area scale (Lifton and Chase, 1992; Hurtrez et al., 1999), the influence of climate (Masek et al., 1994), lithology (Hurtrez et al., 1999), tectonic activity (Ohmori, 1993; Willgoose, 1994; Hurtrez et al., 1999) and erosional processes (runoff or sapping) (Luo, 2000, 2002). It is thus very difficult to discriminate the main factor that controls basin morphometry based on the interpretation of the hypsometric method alone. If we assume that the only predominant factors on early Mars are erosional processes, we infer that Warrego Valles should result from runoff owing to the low hypsometric integral (Luo, 2000, 2002; Grant and Fortezzo, 2003).

### 3.7. Valley longitudinal profiles

The quantitative analysis of individual valleys allows us to determine the local stage of erosion in relation to lithology, tectonics and climate. The valley longitudinal profile is defined by the thalweg as it changes in elevation with increasing valley length. It corresponds to the river incision in response to variations in climate and tectonic effects, local changes in hydraulic parameters (water discharge and load), and lithology.

On Earth, the base level of erosion is an ideal surface reached when there is no aggradation or degradation under static equilibrium. A river is graded when the gradient, width and depth of its channel are in dynamic equilibrium with discharge and load (Mackin, 1948). It is very rare for this to occur and the time-scale for a river to reach equilibrium is very long, e.g. from 1 kyr to 1 Myr (Knox, 1976; Pizzuto, 1992). As most rivers increase in discharge downstream where groundwater and tributaries join together, the typical longitudinal profile is concave-up shaped. In alluvial channels, it is generally accepted that the concave-up longitudinal profile is characteristic of rivers in equilibrium. However, this shape is not a necessary criteria for equilibrium (Sinha and Parker, 1996), and numerous longitudinal profiles along river formed in bedrock show different shapes, although they have reached grade (Pazzaglia et al., 1998). Longitudinal profiles thus give clues for understanding the river adjustments related to climatic, tectonic and lithologic changes on Earth (Merrits et al., 1994).

We analysed four longitudinal profiles extracted from MOLA data in order to estimate the evolution and stage of Warrego Valles (Fig. 15a and b). However, interpretations must be made cautiously because topographic profiles correspond to the present-day which are different than the actual channels that carved the valleys. Indeed, no channel is now observed on images due to degradation and infilling.

The longest valley (B) starts at an elevation of 7.5 km, connects downstream to the main E–W trending tributary (A) at 4.2 km in elevation before continuing 257 km farther to the mouth standing at 2.7 km in elevation. The three others profiles are $<200$ km in length. They developed on a regional topographic slope increasing eastward, from A to D valleys and display a lowly concave-upstream profile, suggesting that they have reached a dynamic equilibrium. However, their downstream longitudinal profile shows a convex-up shape suggesting that either the river developed on resistant rocks (Hack, 1973, 1982), or its downstream discharge decreased (Hack, 1973), or tectonic uplift occurred in the mouth area preventing the river adjustment to reach a graded profile (Hack, 1982; Brookfield, 1998). The latter hypothesis seems the best to explain this morphology in accordance with the image interpretation. In addition, knickpoints are observed along the four longitudinal profiles (Fig. 15b, arrows). They would correspond to the local block uplift due to fault movement. These short convex upward features would have been submitted to the intense erosion and hence attest to the juvenile character of valleys.

Longitudinal profiles are usually interpreted as the result of fluvial processes. Although valley incision results from both surface runoff and groundwater sapping, one of processes is often dominant. For example, the Escalante River located on the Colorado Plateau exhibits two styles of erosion according to both styles of fluvial processes (Laity and Malin, 1985). The valley head area is characterised by a fluvial dendritic pattern related to a concave-up longitudinal profile interpreted as the result of surface runoff erosion. On contrary, the valley mouth area shows a canyon morphology spaced by different knickpoints. The longitudinal profile of this area corresponds to a series of linear segments spaced by steep escarpments.

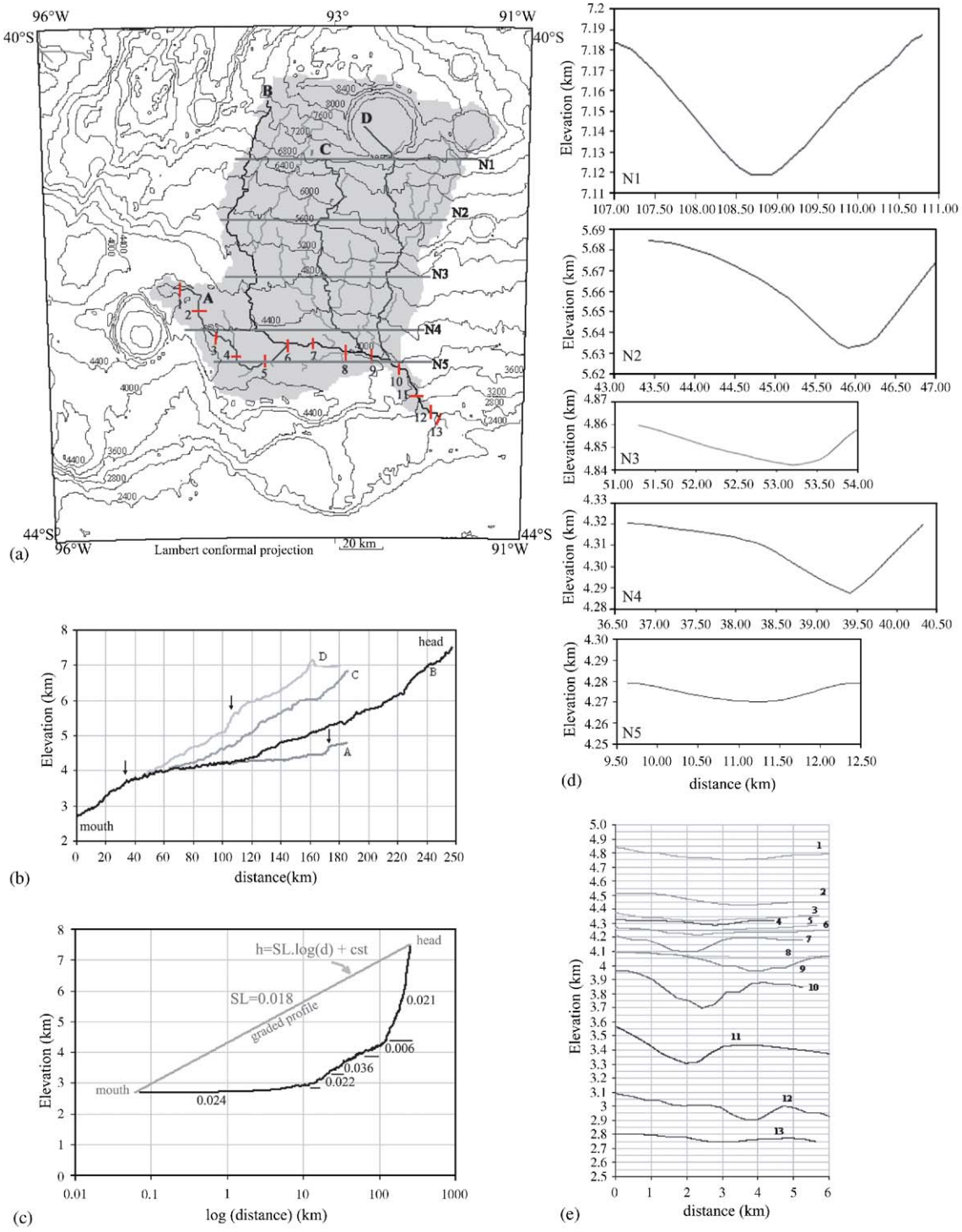


Fig. 15. (a) Locations of topographic cross-sections along and orthogonal to tributaries. (b) Longitudinal profiles of four tributaries (A, B, C and D) in arithmetic graph. Vertical scale is exaggerated 22.5 times. The arrows correspond to the location of knickpoints. (c) Longitudinal profile of the longest tributary (A) in semi-logarithmic graph. The concave-up profile in arithmetic graph becomes a linear one which slope coefficient SL corresponds to Hack's index. The ideal graded profile (grey line) of A tributary is characterised by a low SL index (0.018). The real profile can be cut by linear segments corresponding to segments of graded valley associated with their respective SL index. (d) Examples of transverse profiles crosscutting N–S trending valleys (N1–N5). (e) Transverse profiles crosscutting the main E–W trending tributary from its head to its mouth.

It is interpreted as the result of the head-ward erosion of cliffs helped by sapping of groundwater at their base. If we compare the longitudinal profile of Warrego Valles to that of this terrestrial analogue, we can correlate it to that of the head area of Escalante River and infer that Warrego Valles profile would result from surface runoff at least in its early stage of formation. The knickpoints of Warrego Valles are not associated to a canyon morphology as that observed in

Escalante River. Thus, they would be the result of tectonics associated with possible change in base levels rather than groundwater sapping.

Longitudinal profile can be plotted in semi-logarithmic graph called the Hack's (1973) profile. The altitude of the longest thalweg is plotted as a logarithmic function of the valley length measured from the head to the mouth (Fig. 15c). The concave-up thalweg profile becomes a linear function where the slope coefficient corresponds to the "stream length-gradient index" or "SL index" (Hack, 1973). Most terrestrial channels do not have a single logarithmic profile throughout their length, it consists of connected series of linear segments. In the semi-logarithmic graph, the effect of increasing discharge downstream is masked. The effect of resistance in rivers is shown by the slope of linear segment which is proportional to the size of the bed material or stream power (Hack, 1973). As the SL index is very sensitive to changes in channel slopes, it is applied to assess relationships between tectonic activity, rock resistance and topography (Burnett and Schumm, 1983; Ouchi, 1985).

The Hack's profile of the longest longitudinal profile (A) of Warrego Valles is characterised by a slightly concave-up shape (Fig. 15c) because of the low concavity in linear graph (Fig. 15b). The Hack's profile suggests that Warrego Valles formed in an area of low tectonic activity (Merrits and Vincent, 1989). The concave-up Hack's profile can be cut into several linear segments. Each segment is defined independently by using linear fitting with a correlation coefficient greater than 95%. Each segment expresses a small graded profile with its SL index. Five segments are plotted with their low SL index value close to 0.02. In addition, a straight line is drawn between the head and the mouth of Warrego Valles which may reflect a graded profile in dynamic equilibrium with an SL index value (0.018) deemed to be the proxy of stream power for Warrego Valles. The longest longitudinal profile of Warrego Valles could thus correspond to a small river in terms of stream power owing to its low SL index.

In summary, longitudinal profiles of the main valleys of Warrego Valles are similar to terrestrial ones in a relatively stable tectonic environment, e.g. concave-up shape in head area and a convex-up shape in the mouth area due to regional normal faults. They correspond to profiles of a terrestrial graded valley. They could be explained by the result of both surface runoff and ground sapping. The Hack's profile of the longest tributary is consistent with this interpretation and gives information about the low stream power of river at the origin of valley. This confirms the relative young age of the network obtained from the crater count as Noachian tectonics has not strongly influenced its formation.

### 3.8. Traverse valley profiles

In order to study the geometry of Warrego Valles, we extracted five E–W topographic profiles from the MOLA data, spaced 40 km apart in distance and crosscutting the N–S valleys of Warrego valleys (Fig. 15a). The wide and deep valleys observed in THEMIS IR images are easily detected, but shallow and narrow valleys are nearly indiscernible in the MOLA data. The width of valleys at their top does not increase downstream and has an average width of $3.3 \pm 1.4$ km. The depth of valleys is heterogeneous with a statistical average of $49\,\text{m} \pm 42\,\text{m}$. Note that the valleys often display an asymmetrical V-shape with a higher W-facing slope (Fig. 15d). The west-facing slope is $2.0^\circ \pm 1.5^\circ$ whereas the east-facing slope is $1.6^\circ \pm 1.4^\circ$. Most valleys show a V-shaped profile, which is indicative of surface runoff.

The morphology of the main tributary of Warrego Valles is quite different from that of secondary tributaries (Fig. 15e). Indeed, it is characterised by an opened U-shape profile. A progressive change in shape is observed from west to east with a slightly increase in depth near the mouth (20 m in depth westward to 172 m in depth) before decreasing few meters in depth at the outlet in the southern plains. The large depth corresponds to the river incision close to the tectonic uplift of the outlet area (Fig. 5 and 7). The width remains constant along the main tributary ($3.1 \pm 1.6$ km). The sides of valley show asymmetrical slopes, with a low south-facing slope ($2.6^\circ \pm 2.3^\circ$) and a high north-facing slope ($3.0^\circ \pm 2.8^\circ$). This asymmetry can be due to different erosional processes (gravity instability, etc.) during the valley formation. At a greater scale, this asymmetry could be maintained by mass-sliding and recent ice sublimation correlated with sun exposition (Malin and Edgett, 2000).

In summary, the valley morphology of Warrego Valles is quite common. Martian valleys are usually a few kilometre in width and ~100 m in depth (Williams and Phillips, 2001). We notice that valley width remains constant, but their depth varies. This geometry is quite different from that of terrestrial valleys. Indeed, in the latter, the increase in discharge downstream is related with the increase in valley width from the river head to its mouth, and the V-shape upstream to the U-shape downstream. This constant width of valleys must be interpreted with caution because the transverse profiles are not the pristine ones but may reflect subsequent modifications. Finally, the V-shaped profile of all valleys except the main tributary is indicative of surface runoff.

## 4. What processes formed the valley networks?

Quantitative fluvial geomorphology techniques give excellent descriptions and predictions of drainage networks but no direct explanation about the manner in which they formed. On Earth, river incision results from the external dynamics related to a water cycle. What were the erosive processes on early Mars that created the valley networks ?

Since the valley networks were discovered, a debate has continued about their origin: sapping versus runoff (Sharp and Malin, 1975; Laity and Malin, 1985; Pieri, 1976, 1980;

Baker, 1982, 1990; Baker et al., 1992; Carr, 1981, 1995, 1996; Gulick and Baker, 1989; Grant, 2000; Luo, 2002; Aharonson et al., 2002). On Earth, valleys partially formed by groundwater sapping are located in geological areas characterised by a superposition of permeable rocks resistant to mechanical erosion above impermeable rock easily eroded by groundwater flow. As soon as the sapping occurs, the erosion of permeable rocks is resistant backward into the channel. Consequently, valleys tend to have abrupt, theatre-like terminations and U-shaped cross-sections (Laity and Malin, 1985; Howard, 1988). They tend to maintain their width for long distances downstream because of the low number of tributaries, and they are often arranged in a network with a low drainage density.

In contrast, valleys partially formed by surface runoff are characterised by changes in morphology from head to mouth: narrow and deep, V-shaped cross-section to wide and shallow, and U-shaped cross-section in relation with the increase in discharge downstream (Mackin, 1948). They are arranged in a branch-like pattern characterised by a large drainage density. However, water moving down the slope, called overland flow or direct runoff, is not the only erosive process, except in terrestrial semi-arid or arid regions. Overland flow is associated with water flowing in the unsatured zone above the water table and distinct from groundwater flow. Following intensive rainfall, the combination of the two flows may produce runoff in the form of bank seepage near the channel (Kirkby and Chorley, 1967; Hursh, 1936).

On Mars, groundwater sapping processes may be best represented by the valley morphology of Nirgal or Nanedi Vallis (Carr, 1996). However, many valley networks have geomorphic characteristics consistent with runoff, such as a dendritic, branch-like pattern. However, origin by surface runoff is often not considered because of their low drainage density (Carr and Chuang, 1997). For this reason, Warrego Valles has been interpreted as either the result of groundwater sapping along tectonic fault systems, e.g. Claritas or Thaumasia fossae (Dohm and Tanaka, 1999), or the result of hydrothermal activity and ice/snow melting by magmatic intrusion (Gulick, 1998, 2001). Groundwater sapping along faults could explain the theatre-like features present along wide and deep valleys observed on THEMIS visible image (Fig. 5). However, hydrothermal activity is difficult to reconcile in the formation of a mature valley network system without atmospheric water recharge. Moreover, if we assume that ground contained ice during the Hesperian time (Kargel and Strom, 1992; Clifford, 1993), the ice melting by a magmatic intrusion (Gulick, 2001) appears improbable as there is no magmatic or volcanic structure in the close neighbouring areas of Warrego Valles.

Based on our study, Warrego Valles is best explained by a combination of surface runoff, infiltration, seepage and groundwater flow. Indeed, valley heads are standing at different elevations, e.g. 4–8 km in elevation on the south-facing slope and less than 4 km in elevation on the north-facing slope (Fig. 3). Few wide and deep valleys show theatre-like termination (Fig. 5), which would suggest that sapping processes occurred in some places. Heads of narrow and shallow valleys are characterised by a cone shape, which suggests formation by atmospheric precipitation and surface runoff. In addition, Warrego Valles corresponds to a mature valley network with seven Strahler's orders observed from THEMIS IR images (Fig. 12d). The valley pattern is sub-dendritic to sub-parallel in relation to the local slope (Fig. 12f). Despite its low drainage density ($0.53\,km^{-1}$) in comparison with that of terrestrial networks. Warrego Valles is comparable to a terrestrial network in semi-arid to arid region. Although the present-day morphology of valleys have modified the pristine valleys, it is consistent with that of fluvial valley network formed in an atmospheric water cycle during early Mars (from Noachian to Hesperian times): rainfall or snowfall, surface runoff and seepage (Fig. 16).

An atmospheric water cycle during early Mars is supported by numerous valley networks that incised the Thaumasia highlands and the southern cratered Hesperian plains (Fig. 1). The valley heads are distributed at different

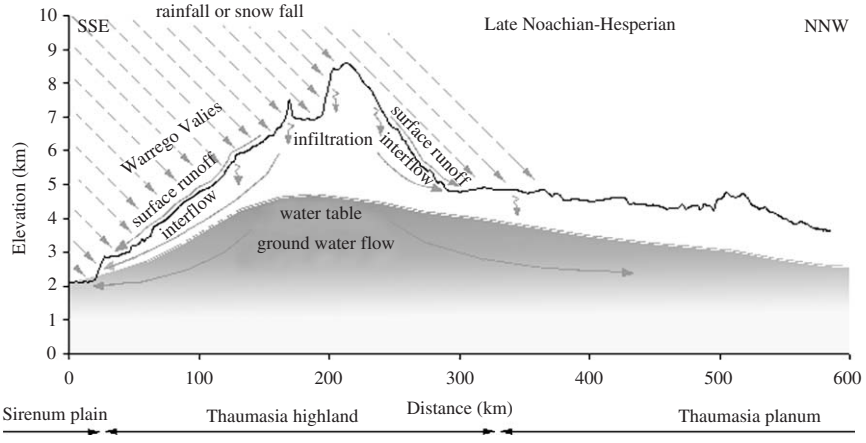


Fig. 16. Sketch for atmospheric water cycle during the Noachian–Hesperian time. Rain or snowfalls occurred on Thaumasia highlands. Water runs off leading to valley formation, and infiltrates leading to recharge water table. If rain or snowfalls were enough important and longer in time, flow, seepage and groundwater flow could also initiate valley erosion.

elevations, e.g. >8 km for Warrego Valles, and also 4 km for the eastern valley networks of Thaumasia highlands (Fig. 1) and 3 km for the western valley networks of Thaumasia highlands. Most of valley networks developed on slope lesser than 5° (Fig. 1d). The distribution of these valley networks is consistent with rainfalls (or snowfalls) that eroded the Martian surface and recharged the water table or aquifer (Craddock and Maxwell, 1993; Craddock and Howard, 2002). Although the snowfalls would do very little erosion on a regional scale, the hypothesis could not be excluded. However, no geomorphic evidence for Hesperian glaciation was observed in this area as snow accumulation zone able to produce glacier and massive amount of erosion. No evidence for fluvial activity due to magmatic heating was found on THEMIS images, because there is no magmatic structure in the close neighbouring areas of Warrego Valles. Moreover, an atmospheric water cycle is supported by the regional distribution of valley networks on the Thaumasia highlands (Fig. 1) and the occurrence of a delta fan in a crater that played the role of ancient lake (Mangold and Ansan, 2004, 2006). The latter implies the occurrence of stable liquid water on a significant duration. All this evidence indicates that Warrego Valles is not an isolated dense network as observed by Viking mapping (Dohm et al., 2001).

## 5. What was the climate on early Mars?

The climate conditions on the early Mars have been debated for three decades due to interpretations of landforms such as valley networks which were controversial at the scale of Viking images. Climate models based on these observations have also been debated, favouring either a pure cold climate (Kasting, 1991) especially due to the lower insolation of the faint sun (Gough, 1981), or potentially a warmer climate sustained by a efficient greenhouse, $CO_2$ clouds and a thicker atmosphere (Pollack et al., 1987; Forget and Pierrehumbert, 1997; Mischna et al., 2000; Colaprete and Toon, 2000). MGS and Mars Odyssey data give us the ability to study features more in detail, quantitatively, and assess the geomorphic parameters that control valley geometry and topography. From these parameters we conclude that a pure subsurface origin for Warrego Valles is unlikely.

Our study strongly favours fluvial processes related to atmospheric precipitation and water cycle including rainfall or meltwater from snow accumulation, subsurface infiltration and drainage (Fig. 16) in agreement with some previous studies (Milton, 1973; Masursky et al., 1977; Pieri, 1980; Carr, 1981; Craddock and Maxwell, 1993; Craddock and Howard, 2002). The distribution of valley networks is consistent with the model of an early, warm and wet Mars (Pieri, 1976; Carr and Chuang, 1997; Craddock and Maxwell, 1993; Craddock and Howard, 2002), in which a water cycle could exist between a vast ocean, atmosphere and continental landforms (Baker et al., 1991). However, questions remain about the duration and magnitude of this warmer period as well as when it ended.

Our study shows that Warrego Valles reached a level of maturity and equilibrium which takes a long time to achieve in terrestrial climates because river incision is a slow process. We estimate that Warrego Valles formed between 1 kyr and 1 Myr in reference to the time of formation of terrestrial valley networks (Knox, 1976; Pizzuto, 1992), depending on precipitation amount. Nevertheless, this duration is still short by comparison to the half billion years during which the network can theoretically develop. The rate of erosion and the amount of eroded material are difficult to determine because it depends both on the amount of precipitation and the properties of the bedrock. Thus, dissection by rivers is especially slow in an arid climate with permeable lava flows or regolith. We also show that there were different periods of activity of the valleys. This suggest that the erosion was episodic rather than continuous over 500 Myr. These effects, taken together, may explain that the Thaumasia highlands are not completely eroded after such a long duration. Episodic warm periods are not improbable as both climates of the Earth and Mars recently exhibits variations due to astronomical parameters (obliquity) and magmatic activity ($CO_2$ increase in atmosphere). One would expect similar climatic variations on early Mars but they are much more difficult to identify and date. But, even episodic the presence of stable liquid water means the occurrence of a thicker atmosphere for the whole period.

Many previous studies have suggested that early Mars experienced intense erosion during the late Noachian through the early Hesperian (Craddock and Maxwell, 1993; Craddock and Howard, 2002), but our study shows the occurrence of significant erosion during the Hesperian epoch, which is usually thought to be cold and dry. This activity is pristine and does not produce most of the erosion seen, but it could be contemporaneous with the formation of other Hesperian valleys, such as those identified on volcanoes (Gulick, 2001), in the Valles Marineris region (Mangold et al., 2004) and Thyrrena region (Mest and Crown, 2004). Our observations suggest that the history of early Mars is much complicated than originally thought and it requires more investigations in order to be fully understood.

## 6. Conclusions

By combining available data sets (Viking, THEMIS IR and visible, MOC images and MOLA altimetry), we can conclude that: (1) Warrego Valles is not isolated on the southern side of Thaumasia highland; (2) Warrego Valles developed in a rectangular-shaped, concave-up drainage basin with numerous valleys on both sides of the main tributary; (3) Warrego Valles is characterised by seven Strahler's orders, and geomorphic parameters, such as a bifurcation ratio equal to 3, a length ratio equal to 1.7, a drainage density equal to 0.53 $km^{-1}$ and a ruggedness

number equal to 3.3, are consistent with a terrestrial fluvial valley network; (4) the distribution of its valleys is highly controlled by slope (parallel pattern on the northern side and dendritic pattern on the central part of Warrego Valles); (5) valley heads are standing at different elevations, which is consistent with runoff processes; (6) the main erosive agent is liquid water as part of an atmospheric water cycle (evaporation, rainfalls/snowfalls, infiltration, seepage and groundwater flows); (7) the hypsometric curve and integral (0.46) indicate that Warrego Valles reached the mature Davis stage; (8) Warrego Valles and the other valley networks on Thaumasia highlands developed by probable successive erosional stages, during Noachian through the late Hesperian; (9) after fluvial activity stopped, valleys underwent modifications by mass wasting, gravity sliding of ice rich material, impact cratering, dust blanketing, etc.

Our study confirms that the early Mars climate was different than the current climate, and supports a fluvial activity and surface runoff. The most recent activity identified as being in Late Hesperian in age suggests that the end of the warmer period is not a simple transition from the end of the Noachian but a more complex transition with a climatic optimum in the Hesperian.

## Acknowledgements

We acknowledge and express our gratitude to Dr. R. Craddock and anonymous reviewer to their constructive review. We thank the Mars Global Surveyor and Mars Odyssey teams for their data. We are grateful to France Ermapper team for her technical help. The Programme National de Planétologie provided support for this study under contract PNP2003.

## References

Abrahams, A.D., 1972. Drainage densities and sediment yields in eastern Australia. Aust. Geogr. Stud. 10, 19–41.

Abrahams, A.D., 1984. Channel networks: a geomorphological perspective. Water Resour. Res. 20, 161–168.

Abrahams, A.D., Ponczynski, J.J., 1984. Drainage density in relation to precipitation intensity in the USA. J. Hydrol. 75, 383–388.

Aharonson, O., Zuber, M.T., Rothman, D.H., Schorghofer, N., Whipple, K.X., 2002. Drainage basins and channel incision on Mars. PNAS 99 (4), 1780–1783.

Ansan, V., Mangold, N., 2003. Warrego Valles revisited using MGS and Odyssey data: valleys formed by precipitations? In: Sixth International Conference on Mars, Pasadena, USA.

Baker, V.R., 1982. The Channels of Mars. University of Texas Press, Austin.

Baker, V.R., 1985. Models of fluvial activity on Mars. In: Woldenberg, M. (Ed.), Models in Geomorphology. Allen & Unwin, Winchester, MA, pp. 287–312.

Baker, V.R., 1990. Spring sapping and valley network development. In: Higgins, C.G., Coates D.R. (Eds.), Groundwater Geomorphology: the Role of Subsurface Water in Earth-Surface Processes and Landform. Geol. Soc. Am. Bull. 252, 235–265 (Special Paper).

Baker, V.R., Kochel, R.C., 1979. Martian channel morphology: Maja and Kasei Valles. J. Geophys. Res. 84, 7961–7983.

Baker, V.R., Partridge, J.B., 1986. Small Martian valleys: pristine and degraded morphologies. J. Geophys. Res. 91, 3561–3572.

Baker, V.R., Strom, R.G., Gulick, V.C., Kargel, J.S., Komatsu, G., Kale, V.S., 1991. Ancient oceans, ice sheets and the hydrological cycle on Mars. Nature 352 (6336), 589–594.

Baker, V.R., Carr, M.H., Gulick, V.C., Williams, C.R., Marley, M.S., 1992. Channels and valley networks. In: Kieffer, H.H., et al. (Eds.), Mars. University of Arizona Press, Tucson, pp. 493–522.

Brookfield, M.E., 1998. The evolution of the great river systems of southern Asia during the Cenozoic India–Asia collision: rivers draining southwards. Geomorphology 22, 285–312.

Burnett, A.W., Schumm, S.A., 1983. Alluvial-river response to neotectonics deformation in Louisiana and Mississippi. Science 222, 49–50.

Cabrol, N.A., Grin, E.A., 2001. Composition of the drainage network on early Mars. Geomorphology 37, 269–287.

Carlston, C.W., 1963. Drainage density and streamflow. US Geol. Surv. Prof. Paper 422C.

Carr, M.H., 1981. Mars. In: Carr, M.H. (Ed.), The Geology of Terrestrial Planets. NASA Special Publications, NASA SP-469, pp. 207–263.

Carr, M.H., 1995. The Martian drainage system and the origin of networks and fretted channels. J. Geophys. Res. 100, 7479–7507.

Carr, M.H., 1996. Water on Mars. In: Carr, M.H. (Ed.). Oxford University Press, New York (229pp).

Carr, M.H., Chuang, F.C., 1997. Martian drainage densities. J. Geophys. Res. 102, 9145–9152.

Carr, M.H., Clow, G.D., 1981. Martian channels and valleys: their characteristics, distribution, and age. Icarus 48, 91–117.

Carr, M.H., Malin, M.C., 2000. Meter-scale characteristics of Martian channels and valleys. Icarus 146, 366–386.

Christensen, P.R., Bandfield, J.L., Bell, J.F., Gorelick, N., Hamilton, V.E., Ivanov, A., Jakosky, B.M., Kieffer, H.H., Lane, M.D., Malin, M.C., McConnochie, T., McEwen, A.S., Mc Sween, H.Y., Mehall, G.L., Moersch, J.E., Nealson, K.H., Rice, J.W., Richardson, M.I., Ruff, S.W., Smith, M.D., Titus, T.N., Wyatt, M.B., 2003. Morphology and composition of the surface of Mars: Mars Odyssey THEMIS results. Science 300 (5628), 2056–2061.

Clifford, S.M., 1993. A model for the hydrologic and climatic behavior of water on Mars. J. Geophys. Res. 98, 10973–11016.

Colaprete, A., Toon, O.B., 2000. The radiative effects of Martian water ice clouds on the local atmospheric temperature profile. Icarus 145, 524–532.

Craddock, R.A., Howard, A.D., 2002. The case for rainfall on a warm, wet early Mars. J. Geophys. Res. 107 (5111), 1–36.

Craddock, R.A., Maxwell, T.A., 1990. Resurfacing of the Martian highlands in the Amenthes and Tyrrhena Region. J. Geophys. Res. 95, 14,265–14,278.

Craddock, R.A., Maxwell, T.A., 1993. Geomorphic evolution of the Martian Highlands through ancient fluvial processes. J. Geophys. Res. 98, 3453–3468.

Dohm, J.M., Tanaka, K.L., 1999. Geology of Thaumasia region, Mars: plateau development, valley origins, and magmatic evolution. Planet. Space Sci. 47, 411–431.

Dohm, J.M., Tanaka, K.L., Hare, T.M., 2001. Geologic map of the Thaumasia region of Mars. US Geol. Surv. Map I-2650.

Duxbury, T.C., Kirk, R.L., Archinal, B.A., Neumann, G.A., 2002. Mars geodesy/cartography working group recommendation on Mars cartographic constants and coordinate systems. In: Symposium on Geospatial Theory, Processing and Application, Ottawa.

Farmer, C.B., Doms, P.E., 1979. Global and seasonal water vapor on Mars and implications for permafrost. J. Geophys. Res. 84, 2881–2888.

Forget, F., Pierrehumbert, R.T., 1997. Warming early Mars with carbon dioxide clouds that scattered infrared radiation. Science 278, 1273–1276.

Garvin, J.B., Sakimoto, S.E.H., Frawley, J.J., Schnetzler, C., 2002. Global geometric properties of Martian impact craters. In: LPSC 33rd, Houston, USA.

Goldspiel, J.M., Squyres, S.W., 2000. Groundwater sapping and valley formation on Mars. Icarus 148, 176–192.
Goldspiel, J.M., Squyres, S.W., Jankowski, D.G., 1993. Topography of small Martian valleys. Icarus 105, 479–500.
Gough, D.O., 1981. Solar interior structure and luminosity variations. Sol. Phys. 74, 21–34.
Grant, J.A., 2000. Valley formation in Margaritifer Sinus, Mars, by precipitation-recharged ground-water sapping. Geology 28, 223–226.
Grant, J.A., Fortezzo, C., 2003. Basin hypsometry on the Earth, Mars, and the Moon. In: Six International Conference on Mars, No. 3050.pdf.
Gregory, K.J., 1976. Drainage networks and climate. In: Derbyshire, E. (Ed.), Climatic Geomorphology. Macmillan, London, pp. 289–315.
Gulick, V.C., 1987. Origin and evolution of valleys on the Martian volcanoes: the Hawaiian analogs. Master's Thesis, University of Arizona, Tucson (146pp).
Gulick, V.C., 1998. Magmatic intrusions and hydrothermal origin for fluvial valleys on Mars. J. Geophys. Res. 103, 19365–19387.
Gulick, V.C., 2001. Origin of the valley networks on Mars: a hydrological perspective. Geomorphology 37, 241–268.
Gulick, V.C., 2004. Another look at valley development on Martian volcanoes. Workshop on Mars Valley Networks, Kohala Coast, Hawaii (4pp).
Gulick, V.C., Baker, V.R., 1989. Fluvial valleys and Martian paleoclimates. Nature 341, 514–516.
Gulick, V.C., Baker, V.R., 1990. Origin and evolution of valleys on Martian volcanoes. J. Geophys. Res. 95, 14325–14344.
Hack, J.T., 1973. Stream profile analysis and stream gradient index. US Geol. Surv. J. Res. 1, 421–429.
Hack, J.T., 1982. Physiographic divisions and differential uplift in the piedmont and blue ridge. US Geol. Surv. Prof. Paper 1265 (49pp).
Hartmann, W.K., Esquerdo, G., 1999. Pathological Martian craters: evidence for a transient obliteration event? Meteorit. Planet. Sci. 34 (2), 159–161.
Hartmann, W.K., Neukum, G., 2001. Cratering chronology and evolution of Mars. Space Sci. Rev. 96 (1–4), 165–194.
Head, J.W., Mustard, J.F., Kreslavsky, M.A., Milliken, R.E., Marchant, D.R., 2003. Recent ice ages on Mars. Nature 426, 797–802.
Horton, R.E., 1945. Erosional development of streams and their drainage basin. Hydrophysical approach to quantitative morphometry. Geol. Soc. Am. Bull. 56, 275–370.
Howard, A.D., 1988. Sapping features of the Colorado Plateau. In: Howard, A.D., Kochel, R.C., Holt, H.E. (Eds.), A Comparative Planetary Geology Field Guide. NASA SP-491, p. 108.
Hursh, C.R., 1936. Storm-water and absorption. Am. Geophys. Union Trans. 17, 301–302.
Hurtrez, J.E., Sol, C., Lucazeau, F., 1999. Effect of drainage area on hypsometry from an analysis of small-scale drainage basins in the Siwalik Hills (central Nepal). Earth Surf. Process Landf. 24, 799–808.
Kargel, J.S., Strom, R.G., 1992. Ancient glaciation on Mars. Geology 20, 3–7.
Kasting, J.F., 1991. $CO_2$ condensation and the climate of early Mars. Icarus 94, 1–13.
Kirk, R.L., Archinal, B.A., Lee, E.M., Davies, M.E., Colvin, T.R., Duxbury, T.C., 2001. Global digital image mosaics of Mars: assessment of geodetic accuracy. In: LPSC XXXII, No. 1856.pdf.
Kirkby, M.J., Chorley, R.J., 1967. Throughflow, overland flow, and erosion. Int. Assoc. Sci. Hydrol. Bull. 12, 5–21.
Kochel, R.C., 1985. Surface morphology of valley networks formed by sapping. In: LPSC XVI, Houston, TX, pp. 441–442.
Knox, J.C., 1976. Concept of the graded stream. In: Melhorn, W., Flemal, R. (Eds.), Theories of Landform Development. George Allen & Unwin, London, pp. 168–198.
Leighton, R.B., Murray, B.C., Sharp, R.P., Allen, J.D., Sloan, R.K., 1965. Mariner IV photography of Mars: initial results. Science 149, 627–630.
Laity, J.E., Malin, M.C., 1985. Sapping processes and the development of theater-headed valley networks in the Colorado Plateau. Geol. Soc. Am. Bull. 96, 203–217.
Lifton, N.A., Chase, C.G., 1992. Tectonic, climatic and lithologic influences on landscape fractral dimension and hypsometry: implications for landscape evolution in the San Gabriel Mountains, California. Geomorphology 5, 77–114.
Loesch, T.N., 2001. Hydrologic analysis using GIS. Minnesota GIS/LIS Consortium. Spring Workshops, Alexandria, MN.
Luo, W., 2000. Quantifying ground-water-sapping landforms with a hypsometric technique. J. Geophys. Res. 105, 1685–1694.
Luo, W., 2002. Hypsometric analysis of Margaritifer Sinus and origin of valley networks. J. Geophys. Res. 107 (5071), 1–10.
Mackin, J.H., 1948. Concept of the graded stream. Geol. Soc. Am. Bull. 59, 463–512.
Malin, M.C., Carr, M.H., 1999. Groundwater formation of Martian valleys. Nature 397, 589–591.
Malin, M.C., Edgett, K.S., 2000. Evidence for recent groundwater seepage and surface runoff on Mars. Science 288, 2330–2335.
Malin, M.C., Carr, M.H., Danielson, G.E., Davies, M.E., Hartmann, W.K., Ingersoll, A.P., James, P.B., Masursky, H., McEwen, A.S., Soderblom, L.A., Thomas, P., Veverka, J., Caplinger, M.A., Ravine, M.A., Soulanille, T.A., Warren, J.L., 1998. Early views of the Martian surface from the Mars Orbiter Camera of Mars Global Surveyor. Science 279, 1681–1685.
Mangold, N., 2003. Geomorphic analysis of lobate debris aprons on Mars at Mars Orbiter Camera scale: evidence for ice sublimation initiated by fractures. J. Geophys. Res. 108, 8021.
Mangold, N., Ansan, V., 2004. Long Term Stability of Water on Early Mars from the Identification of Lakes and Deltas on Mars. EGU, Nice, France.
Mangold, N., Ansan, V., 2006. Detailed study of an hydrological system of valleys, a delta and lakes in the Southwest Thaumasia region, Mars. Icarus 180, 75–87.
Mangold, N., Quantin, C., Ansan, V., Delacourt, C., Allemand, P., 2004. Evidence for precipitation on Mars from dendritic valleys in the Valles Marineris area. Science 305 (5680), 78–81.
Mars Channel Working Group, 1983. Channels and valleys on Mars. Geol. Soc. Am. Bull. 94, 1035–1054.
Masek, J.G., Isacks, B.L., Gubbels, T.L., Fielding, E.J., 1994. Erosion and tectonics at the margins of continental plateaus. J. Geophys. Res. 99, 13941–13956.
Masursky, H., Boyce, J.M., Dial, A.D., Schaber, G.G., Strobell, M.E., 1977. Classification and time formation of Martian channels based on Viking data. J. Geophys. Res. 82, 4016–4038.
Melton, M.A., 1958. Correlation structure of morphometric properties of drainage systems and their controlling agents. J. Geol. 66, 442–460.
Merrits, D., Vincent, K.R., 1989. Geomorphic response of coastal streams to low, intermediate and high rates of uplift, Mendocino Triple Junstion region, Northern California. Geol. Soc. Am. Bull. 110, 1373–1388.
Merrits, D.J., Vincent, K.R., Wohl, E.E., 1994. Long river profiles, tectonism and eustay: a guide to interpreting fluvial terraces. J. Geophys. Res. 99 (B7), 14031–14050.
Mest, S.C., Crown, D.A., 2004. Morphologic and morphometric analyses of fluvial systems in the southern highlands of Mars. Workshop on Mars Valley Networks, Kohala Coast, Hawaii.
Milton, D.J., 1973. Water and processes of degradation in the Martian landscape. J. Geophys. Res. 78, 4037–4047.
Mischna, M.A., Kasting, J.F., Pavlov, A., Freedman, R., 2000. Influence of carbon dioxide on early Martian climate. Icarus 145, 546–554.
Morgan, R.P.C., 1973. The influence of the scale in climatic geomorphology: a case study of drainage density in Western Malaysia. Geogr. Ann. 55A, 107–115.
Mustard, J.F., Cooper, C.D., Rifkin, M.K., 2001. Evidence for recent climate change on Mars from the identification of youthful near-surface ground ice. Nature 412, 411–414.
Ohmori, H., 1993. Changes in the hypsometric curve through mountain building resulting from concurrent tectonics and denudation. Geomorphology 8, 263–277.

Ouchi, S., 1985. Response of alluvial rivers to slow active tectonic movement. Geol. Soc. Am. Bull. 96, 504–515.

Patton, P.C., Baker, V.R., 1976. Morphometry and floods in small drainage basins subject to diverse hydrogeomorphic controls. Water Resour. Res. 12, 941–952.

Pazzaglia, F., Gardener, T., Merrits, D., 1998. Bedrock fluvial incision and longitudinal profile development over geologic time scales determined by fluvial terraces. In: Tinkler, K., Wohl, E. (Eds.), River Over Rock: Fluvial Processes in Bedrock Channels. American Geophysical Union, Washington, DC, pp. 207–235.

PDS web site: 〈http://pdsmaps.wr.usgs.gov/PDS/public/explorer/html/mdim2.htm〉.

Pieri, D.C., 1976. Martian channels: distribution of small channels on the Martian surface. Icarus 27, 25–50.

Pieri, D.C., 1980. Martian valleys: morphology, distribution, age and origin. Science 210, 895–897.

Pizzuto, J.E., 1992. The geomorphology of graded gravel rivers: a network perspective. Geomorphology 5, 457–474.

Phillips, L.O., Schumm, S.A., 1987. Effect of regional slope on drainage networks. Geology 15, 813–816.

Pollack, J.B., Kasting, J.F., Richardson, S.M., Poliakoff, K., 1987. The case for a wet, warm climate on early Mars. Icarus 71, 203–224.

Ritter, D.L., Kochel, R.C., Miller, J.R. (Eds.), 2002. Process Geomorphology. McGraw-Hill, Boston, p. 560.

Sagan, C., Toon, O.B., Gierasch, P.J., 1973. Climatic change on Mars. Science 181, 1045–1049.

Schultz, P.H., Ingerson, F.E., 1973. Martian lineaments from Mariner 6 and 7 images. J. Geophys. Res. 78, 8415–8427.

Schultz, R.A., Tanaka, K.L., 1994. Lithospheric scale buckling and thrust structures on Mars: the Coprates rise and south Tharsis ridge belt. J. Geophys. Res. 99, 8371–8385.

Schumm, S.A., 1956. Evolution of drainage systems and slopes in badlands at Perth Amboy, New Jersey. Geol. Soc. Am. Bull. 67, 597–646.

Schumm, S.A., Mosley, M.P., Weaver, W.E. (Eds.), 1987. Experimental Fluvial Geomorphology. Wiley, New York, p. 413.

Seidelmann, P.K., Abablakin, V.K., Bursa, M., Davies, M.E., De Bergh, C., Leiske, J.H., Oberst, J., Simon, J.L., Standish, E.M., Stooke, P., Thomas, P.C., 2002. Report of the IAU/IAG working group on cartographic coordinates and rotational elements of the planets and satellites: 2000. Celest. Mech. Dyn. Astron. 82, 83–110.

Sharp, R.P., Malin, M.C., 1975. Channels on Mars. Geol. Soc. Am. Bull. 86, 593–609.

Sinha, S.K., Parker, G., 1996. Causes of concavity in longitudinal profiles of rivers. Water Resour. Res. 32, 1417–1428.

Smith, D.E., 1998. The global topography of Mars and Implications for surface evolution. Science 284 (5422), 1932.

Smith, D.E., Zuber, M.T., Solomon, S.C., Phillips, R.J., Head, J.W., Garvin, J.B., Banerdt, W.B., Muhleman, D.O., Pettengill, G.H., Neumann, G.A., Lemoine, F.G., Abshire, J.B., Aharonson, O., Brown, C.D., Hauck, S.A., Ivanov, A.B., Mc Govern, P.J., Zwally, H.J., Duxbury, T.C., 1999. The global topography of Mars and Implications for surface evolution. Science 284, 1495–1503.

Smith, D.E., Zuber, M.T., Frey, H.V., Garvin, J.B., Head, J.W., Muhleman, D.O., Pettengill, G.H., Phillips, R.J., Solomon, S.C., Zwally, H.J., Banerdt, W.B., Duxbury, T.C., Golombeck, M.P., Lemoine, F.G., Neumann, G.A., Rowlands, D.D., Aharanson, O., Ford, P.G., Ivanov, A.B., Johnson, C.L., McGovern, P.J., Abshire, J.B., Afzal, R.S., Sun, X., 2001. Mars Orbiter Laser Altimeter: experiment summary after the first year of global mapping of Mars. J. Geophys. Res. 106, 23689–23722.

Squyres, S.W., 1989. Urey price lecture: water on Mars. Icarus 79, 229–288.

Squyres, S.W., Clifford, S.M., Kuzmin, R.O., Zimbelman, J.R., Costard, F.M., 1992. Ice in the Martian regolith. In: Kieffer, H.H., et al. (Eds.), Mars. University of Arizona Press, Tucson, pp. 523–556.

Stepinski, T.F., Collier, M.L., 2003. Drainage densities of computationally extracted Martian drainage basins. In: Sixth International Conference on Mars, No. 3100.pdf.

Strahler, A.N., 1952a. Dynamic basis of geomorphology. Geol. Soc. Am. Bull. 63, 923–938.

Strahler, A.N., 1952b. Hypsometric (area-altitude) analysis of erosional topography. Geol. Soc. Am. Bull. 63, 1117–1142.

Strahler, A.N., 1968. Quantitative geomorphology. In: Fairbridge, R.W. (Ed.), Encyclopaedia of Geomorphology. Reinhold, New York, pp. 898–912.

Strom, R.G., Croft, S.K., Barlow, N.G., 1992. The Martian impact cratering record. In: Kieffer, H.H., et al. (Eds.), Mars. University of Arizona Press, Tucson, pp. 383–423.

Tanaka, K.L., 1986. The stratigraphy of Mars. J. Geophys. Res. 91, E139–E158.

Tanaka, K.L., Dohm, J.M., Lias, J.H., Hare, T.M., 1998. Erosional valleys in the Thaumasia region of Mars: hydrothermal and seismic origin. J. Geophys. Res. 103, 31407–31420.

Vincendon, C., Mangold, N., Masson, P., Ansan, V., 2002. Estimation of dust thickness in Arabia Terra region. In: LPSC 33th, Houston, USA.

Willgoose, G., 1994. A physical explanation for an observed area–slope–elevation relationship for catchments with declining relief. Water Resour. Res. 30, 151–159.

Williams, R.M.E., Phillips, R.J., 2001. Morphometric measurements of Martian Valley networks from Orbiter Laser Altimeter (MOLA) data. J. Geophys. Res. 106 (E10), 23737–23751.

Zuber, M., Smith, D.E., Solomon, S.C., Muhleman, D.O., Head, J.W., Garvin, J.B., Abshire, J.B., Bufton, J.L., 1992. The Mars Observer laser altimeter investigation. J. Geophys. Res. 97, 7781–7797.